Inter-hemispheric temperature gradient and equatorial Pacific SSTs drive Sahel monsoon uncertainties under global warming

Marcellin Guilbert[a], Pascal Terray[a], Juliette Mignot[a], Luther Ollier[a], Guillaume Gastineau[a]

[a] *Laboratoire d'Océanographie et du Climat: Expérimentations et Approches Numériques, Institut Pierre-Simon Laplace, Sorbonne Université/CNRS/IRD/MNHN, Paris, France*

Corresponding author: Marcellin Guilbert, marcellin.guilbert@locean.ipsl.fr

ABSTRACT

The Sahel is one of the most vulnerable regions to climate change. Robust estimation of future changes in the Sahel monsoon is therefore essential for effective climate change adaptation. Unfortunately, state-of-the-art climate models show large uncertainties in their projections of Sahel rainfall. In this study, we use 32 models from CMIP6 to identify the sources of this large inter-model spread of Sahel rainfall.

By using Maximum Covariance Analysis, we first highlight two new key drivers of this spread during boreal summer: the inter-hemispheric temperature gradient and equatorial Pacific Sea Surface Temperature (SST) changes. This contrasts with previous studies, which have focused mainly on the Northern Hemisphere rather than the global scale, and in which the Pacific Ocean has been neglected in favor of the Atlantic. Next, we unravel the physical mechanisms behind these statistical relationships. Firstly, the modulation of the inter-hemispheric temperature gradient across the models leads to varying latitudinal positions of the Inter Tropical Convergence Zone and, consequently, varying Sahel rainfall intensity. Secondly, models that exhibit less warming than the Multi-Model Mean in the equatorial Pacific, thereby projecting a less "El Niño-like" mean state, simulate enhanced precipitation over the central Sahel in the future through modulations of the Walker circulation, the Tropical Easterly Jet, the meridional tropospheric temperature gradient, and hence regional zonal wind shear. Finally, we show that these two indices collectively explain 62% of Sahel rainfall change uncertainty: 40% due to the inter-hemispheric temperature gradient and 22% through equatorial Pacific SST.

KEYWORDS : MONSOON, CLIMATE CHANGE, TELECONNECTIONS, MODEL UNCERTAINTY

Early Online Release: This preliminary version has been accepted for publication in *Journal of Climate*, may be fully cited, and has been assigned DOI 10.1175/JCLI-D-23-0162.1. The final typeset copyedited article will replace the EOR at the above DOI when it is published.

1. Introduction

The Sahel experiences a rainy season from June to September (JJAS) associated with the northward migration of the InterTropical Convergence Zone (ITCZ) (Nicholson 2013a), while the rest of the year is practically entirely dry. The Sahel monsoon is characterized by a complex vertical structure of the atmospheric circulation (Shekhar and Boos 2017; Akinsanola and Zhou 2019). In the lower troposphere, southwesterly winds bring moisture from the tropical Atlantic (Sultan and Janicot 2003), while, in the middle (500 hPa) and upper troposphere (200 hPa), the circulation is dominated, respectively, by the African Easterly Jet (AEJ) and the Tropical Easterly Jet (TEJ, Nicholson 2009). The Sahel monsoon provides most of the water resources for predominantly rainfed agriculture, which is the main source of income for the region (Sultan and Gaetani 2016). Coupled with the exponential growth of the population and the ongoing desertification process (Wei et al. 2017), Sahel is one of the most vulnerable places to climate change in the world (Sylla et al. 2016).

The long-lasting Sahel drought in the 1970s and 1980s has offered a glimpse of the potential climate impacts of human activities on this region. Indeed, many studies have established the existence of a human-induced component in the drought, mainly related to land surface atmosphere feedbacks (Charney et al. 1975; Kucharski et al. 2013) and anthropogenic aerosols (Dong and Sutton 2015; Giannini and Kaplan 2019; Ndiaye et al. 2022). The latter have an impact on Sahel rainfall through the anomalous inter-hemispheric radiative imbalance they induce (Hwang et al. 2013; Schneider et al. 2014) and via their effects on anomalous Sea Surface Temperature (SST) patterns, especially in the Atlantic Ocean (Giannini and Kaplan 2019; Hirasawa et al. 2020). However, as the internal component of the Atlantic Multidecadal Oscillation can lead to similar anomalous SST patterns (Martin and Thorncroft 2014) and a partial recovery of the West African Monsoon (WAM) has been observed since the early 2000s (Lebel and Ali 2009), the magnitude of the human-induced component of the 1980s drought is still hotly debated (Janicot et al. 2015). At the same time, the reduction in aerosols emissions around the North Atlantic that resulted from environmental legislation during the 1980s (Seth et al. 2019; Biasutti 2019), combined to their short atmospheric lifetime, may also have reversed the anomalous inter-hemispheric radiative imbalance (Giannini and Kaplan 2019) and thereby played a role in the recent recovery. While most studies focus on the Atlantic, Park et

Accepted for publication in *Journal of Climate*. DOI 10.1175/JCLI-D-23-0162.1.

al. (2016) suggest that rising SSTs in the Mediterranean may also be a driver in the Sahel monsoon recovery.

Finally, greenhouse gasses (GHGs) emissions could have also contributed to the observed modulations, yet with two opposing effects (Chou and Neelin 2004; Marvel et al. 2020; Monerie et al. 2022). On the one hand, by increasing the specific humidity according to the Clausius-Clapeyron relationship and by promoting a warmer Sahara and a stronger Sahara Heat Low (SHL; Cook and Vizy 2015; Wei et al. 2017; Dixon et al. 2018; Terray et al. 2018; Sooraj et al. 2019), GHG forcing could increase local precipitation by promoting low-level moisture convergence and shifting the rainbelt northward in a warming climate (Dixon et al. 2018; Byrne et al. 2018; Terray et al. 2018; Sooraj et al. 2019). On the other hand, the stabilization of the tropical troposphere and the dry air intrusions induced by a strengthening of the associated Saharan shallow meridional circulation linked to a stronger SHL and the GHGs could make convection more difficult in this transition zone (Chou and Neelin 2004; Biasutti 2013; Shekhar and Boos 2017; Hill 2019). Thus, GHGs forcing promotes several contradictory effects, primarily in terms of dynamical response partly mediated by the complex role of the SHL in the WAM (Biasutti 2013; Dixon et al. 2018; Hill 2019), but also through interactions between the dynamic and thermodynamic responses (Chen et al. 2020).

In a nutshell, the historical period illustrates that there are many factors potentially influencing the Sahel rainfall, each with different and sometimes contradictory effects, ranging from regional to global scales. This complexity might be partly reflected in the substantial disagreement between coupled model projections, persisting from Coupled Model Intercomparison Project (CMIP) 3 to CMIP6, with an inter-model spread larger than the multi-model mean (MMM) change, and some CMIP models projecting a drying and others a wettening of the Sahel (Monerie et al. 2017b; Zhang and Li 2022). As the forcing at the end of the 21st century is dominated by GHGs, the large inter-model spread probably comes mainly from the opposing GHG effects described above (Biasutti 2019). More specifically, studies suggest that the main source of inter-model spread in the projections does not seem to come from the thermodynamic response, but rather from the dynamic one, for which climate models have difficulty in reaching a robust agreement (Kent et al. 2015; Monerie et al. 2020b; Zhang

Accepted for publication in *Journal of Climate*. DOI 10.1175/JCLI-D-23-0162.1.

and Li 2022). This dynamical disagreement among models' projections has been mainly linked to teleconnections arising from anomalous SSTs in various oceanic basins, but also to the persistent difficulties of CMIP coupled models to capture realistically the main processes driving the WAM (Roehrig et al. 2013). Park et al. (2015) and Monerie et al. (2020b) suggested that the spread in the relative warming between the Northern Hemisphere and the Tropics modulates the strength of the SHL and the low-level monsoon circulation. Some studies specifically highlight the role of individual oceanic basins. Regarding the Atlantic Ocean, it is suggested that differential warming between the tropical and North Atlantic regions is a key player (Zhang and Li 2022). Beyond its role in the revival of the Sahel monsoon in the recent decades, Park et al. (2016) also identified Mediterranean warming as a key factor in shaping the future of the Sahel monsoon. Finally, a link between model biases in various regions of the world over the current period and the inter-model spread of the future Sahel monsoon has also been put forward by several studies (Roehrig et al. 2013; Yan et al. 2019). As an illustration, Yan et al. (2019) indicate a strong relationship between the uncertainties of future Sahel monsoon rainfall and the inter-model spread of summer precipitation biases in South Asia and the North-West Pacific (NWP), suggesting that this relationship stem from the diversity of deep convection parameterizations used by the models.

In this study, we use Maximum Covariance Analysis (MCA) to objectively analyze the relationships between the projected Sahel rainfall and projected global surface temperatures and rainfall (including both land and ocean) across CMIP6 models. The underlying questions are : 1) Can we revisit the factors explaining the projected Sahel rainfall uncertainties from an objective analysis of the projected changes at the ocean-atmosphere-land surface ? 2) By what physical processes are these factors related to Sahel rainfall? 3) How much uncertainty can they explain?

Section 2 describes models and analysis methods used in this study. Section 3 provides a systematic evaluation of the statistical relationship between the inter-model spread of Sahel rainfall and global surface temperature and rainfall changes by the end of the 21st century in the CMIP6 models. Section 4 examines the physical processes linking the influencing large-scale drivers and regions found in Section 3 to Sahel rainfall, the amount of uncertainty they explain and their respective individual contributions to it. The last section presents a summary and future perspectives.

Accepted for publication in *Journal of Climate*. DOI 10.1175/JCLI-D-23-0162.1.

2. Data and methods

a) *Coupled simulations, validation datasets and climate indices*

This study is based on the high emission Shared Socio-economic Pathways 8.5 (SSP5-8.5) scenario experiments, and uses outputs of 32 CGCMs from CMIP6 (see supplementary Table S1; Eyring et al. 2016). The monthly mean outputs used in our analysis are rainfall (Pr), surface temperature (Ts), near-surface air temperature (Tas), Sea Level Pressure (SLP), horizontal winds (U and V) and geopotential (Zg) at different levels. Here, in most of our statistical analyses, we use only one simulation member for each model, but we also checked in a preliminary step that our main MCA results are not sensitive to the multi-members averaging, which imply that the inter-model spread is largely driven by differences in the forced response of the models in our analysis framework (see Sections 2b, 4a, Fig. 3 and S3 for more details).

Table 1 summarizes the different climate indices and regions used in our analysis. In addition to definitions of the whole Sahel region, or parts of it (Monerie et al. 2021), it includes the canonical Nino3.4 index, a Northern Hemisphere differential warming and a northern minus tropical Atlantic SST index all defined in previous studies as important drivers of the Sahel rainfall changes (Park et al. 2015; Monerie et al. 2020a; Zhang and Li 2022). It also includes an interhemispheric temperature defined with respect to the latitude 15°N because our focus is on the boreal summer season (e.g., from June to September). However, our results remain valid if we define this gradient with respect to the Equator instead (not shown). Finally, defining the interhemispheric gradient from 75°S to 75°N yields very similar results; it is therefore not sensitive to very high latitudes.

A tropospheric thickness gradient is also introduced and will be used in Section 5b when discussing the influence of the equatorial Pacific on the TEJ and the meridional tropospheric temperature gradient in the african-asian sector.

Accepted for publication in *Journal of Climate*. DOI 10.1175/JCLI-D-23-0162.1.

Regions / Indices	Domain and variable used when relevant
Canonical Sahel	[10N;20N], [20W;20E], land only
Extended Sahel	[3N;20N], [20W;20E], land only
Western Sahel	[10N;20N], [20W;5W], land only
Central Sahel	[10N;20N], [5W;20E], land only
Niño3.4	$< SST >_{[5S;5N],\,[170W,120W]}$
Inter-hemispheric temperature gradient	$< Ts >_{[15N;90N],[0;360]} - < Ts >_{[90S;15N],[0;360]}$
Northern Hemisphere differential warming	$< SST >_{[30N;75N],[0;360]} - < SST >_{[20S;20N],[0;360]}$
Northern minus tropical Atlantic SST change	$< SST >_{[45N;65N],[40W;10W]} - < SST >_{[20S;10N],[40W;10W]}$
Thickness gradient around Sahel	$< Zg^{200hPa}\text{-}Zg^{850hPa} >_{[20N;30N],[20W;20E]} - < Zg^{200hPa}\text{-}Zg^{850hPa} >_{[0;10N],[20W;20E]}$

TABLE 1. Definition of the indices used in the present study. < > stands for spatial averaging of the corresponding variable over the subscript domain. The superscript indicates the surface type or the atmospheric level over which the average is taken, when relevant.

b) Methods

Our analysis will focus on June-September (JJAS) as the rainy season for the Sahel in both the historical and future simulations. Note that this departs from the usual definition, JAS, which is commonly used for observations (Sultan and Janicot 2003). However, as the length or the onset of the WAM may vary substantially across the models or the target period, we have decided to use JJAS as the canonical rainy season in order to be sure that we don't miss any rainfall signal across the models or the different simulations in our analysis. We define the

Accepted for publication in *Journal of Climate*. DOI 10.1175/JCLI-D-23-0162.1.

change of a given variable associated with global warming as the difference between the future climatology defined over the period [2064-2099], using SSP5-8.5 experiment, and the present simulated climatology computed over the period [1979-2014], using historical experiment. In the following, all changes are normalized by the corresponding global mean surface temperature increase for each model, so that we look at responses for a same level of warming among models. This choice will be discussed in more details and validated in Section 4. All datasets were interpolated onto a common 2.8°x2.8° horizontal resolution by bilinear interpolation prior to the analysis, which is the coarsest spatial resolution among the 32 models. Velocity potential used in Section 5 is calculated at different levels from horizontal winds with the spectral method (Tanaka et al. 2004).

In order to investigate the first order linear relationships between changes seen from climate indices, we use scatter plots and correlation/regression analyses across the various models. P-values of correlations are calculated using Student t-test with 31 degrees of freedom, given the use of 32 GCMs and thus assuming that they are independent. Yet, for a more systematic exploration, we use MCA, which extracts the dominant co-variability patterns from two geophysical datasets (Bretherton et al. 1992; Cherry 1997). This method has the advantage of not using a rainfall index such as the Sahel rainfall mean, so we make no assumptions about how monsoon rains are spatially modulated in the Sahel. In the following sections, we will call the expansion coefficient model series of the two fields estimated from each MCA mode, the Singular Variable (SV) model series and these SV series are always normalized. The associated spatial patterns are derived by regressing the two fields upon these different normalized SVs. These spatial patterns are homogeneous and heterogeneous maps in the terminology of Bretherton et al. (1992) depending if the SV is from the same field or not. Thus, these maps have the same units and represent typical amplitude anomalies of the two fields associated with the mode.

We will use quantities such as the correlation (r) between the expansion coefficient model series of the two fields, the Squared Covariance Fraction (SCF) and Normalized root-mean-square Covariance (NC) to assess the relevance of a particular MCA mode. The SCF statistic is an indicator of the relative importance of different modes within the same MCA, while the NC is a metric that allows us to compare the importance of modes from different MCAs. More comprehensive details about the MCA and its metrics are given in supplementary Text S1. We compute the significance of the MCA statistics (e.g., r, SCF and NC) by using a bootstrap

Accepted for publication in *Journal of Climate*. DOI 10.1175/JCLI-D-23-0162.1.

resampling MCA scheme with 500 shuffles (e.g., in each shuffle, the rows of one of the matrix fields are randomly permuted before recomputing the covariance matrix and the MCA). The idea is to generate a large number of independent realizations of the covariance matrix under the assumption that the two fields are independent of each other in order to assess the confidence level of the obtained signal as seen by the MCA statistics.

To capture the entire main mode of Sahel precipitation change with the MCA, we use an extended region compared to the canonical Sahel definition, called "extended Sahel" in Table 1. This enables us to better capture the meridional shifts of the ITCZ than over the canonical Sahel region. Note, however, that the first MCA modes obtained by using the canonical or extended boxes are almost identical (r=0.99), illustrating the robustness of the leading MCA patterns with respect to the choice of the Sahel boundaries.

Finally, in Section 5, we use three statistical methods to estimate the relative contributions of the different factors that explain the inter-model spread in rainfall change over the Sahel. First, we use a Permutation Feature Importance (PFI) method (Fisher et al. 2019) to get a measure of how much the accuracy of the regression model depends on the information in each input variable. Technically, all variables are held constant except one for which random permutations are made. The difference in the Sum of Squared Residuals (SSR) between the output of the regression model when using the initial input data versus the randomly permuted variable is evaluated. This is repeated 10,000 times for each variable and the median of the SSR distributions for each variable are compared to obtain the relative contribution of the given input data. Second, we construct a Random Forest model fitting the data. We also use a similarity measure of variable importance (Breiman 2001) to assess the results of our first method. From each constructed tree, we randomly permute one of the input variables and run down the corresponding tree. Then, we compare the resulting output with the correct one to get a mis-regression rate. This is similar to the PFI method, but adapted to the method of random forest. Thirdly and finally, we use a Dominance Analysis (Azen and Budescu 2003), which computes the variable's individual effect as well as its effect in the presence of other variables to identify its relative contribution to the full regression model. For bilinear regression, this corresponds to the average between the individual contribution and the incremental contribution resulting from the interactions with the other factor.

Accepted for publication in *Journal of Climate*. DOI 10.1175/JCLI-D-23-0162.1.

3. Global changes of surface temperature and precipitation over the 21st century

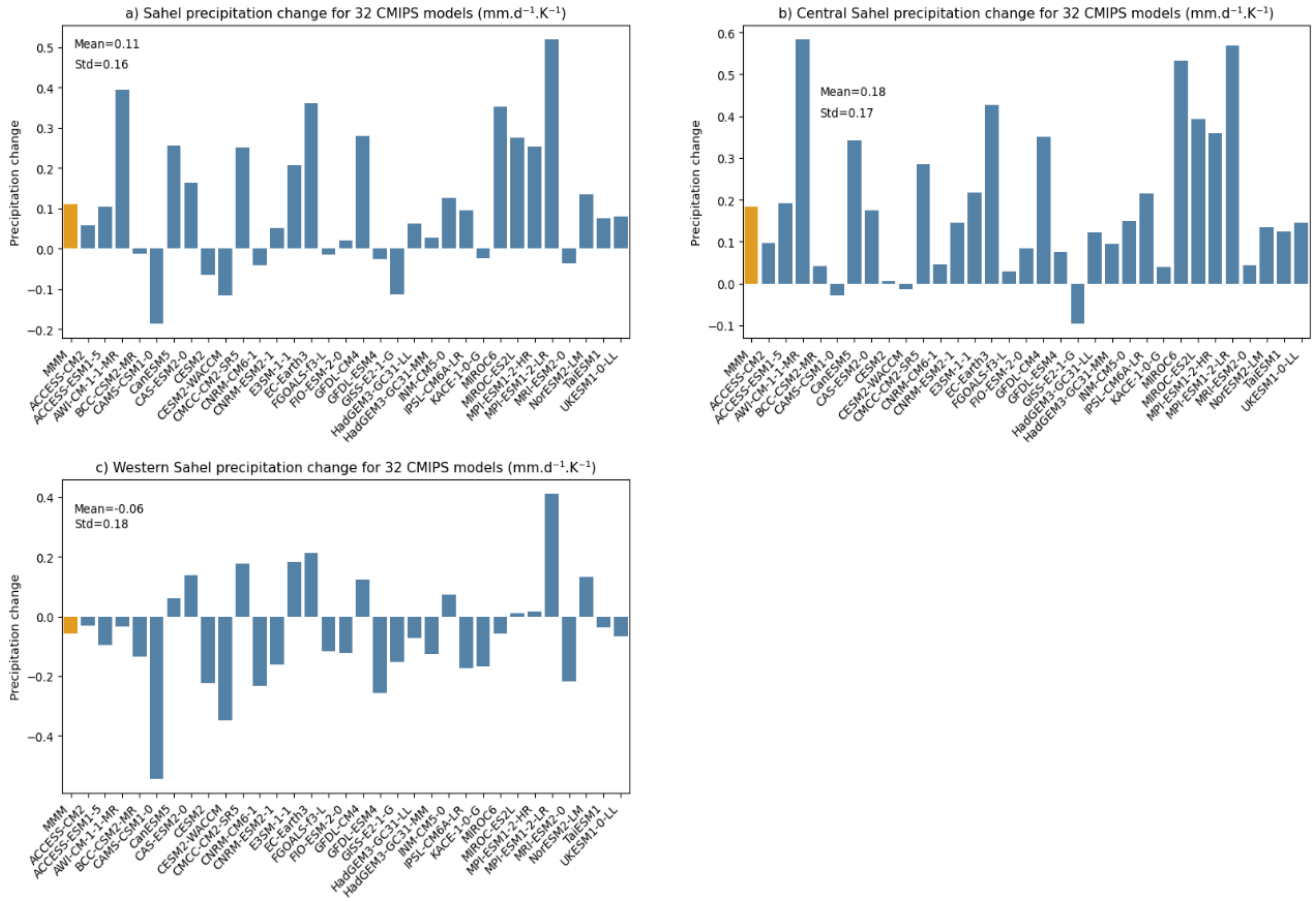

Fig. 1. Rainfall change (JJAS) computed on (a) the Sahel canonical domain, (b) Central Sahel and (c) Western Sahel for 32 CMIP6 models and their MMM (left orange bar). All the model changes are scaled by the global surface temperature change in each model as explained in Section 2. Units is mm.d^{-1}.K^{-1}. See Table 1 for indices definitions.

In agreement with previous studies (Monerie et al. 2017b; Zhang and Li 2022), Fig.1 illustrates that CMIP6 models show a wide range of responses of the Sahel monsoon to climate change towards the end of the 21st century in the SSP5-8.5 simulations. The MMM (0.11 mm.d-¹.K-

Accepted for publication in *Journal of Climate*. DOI 10.1175/JCLI-D-23-0162.1.

$^{-1}$) results from an increase in precipitation over the central Sahel (MMM=0.18 mm.d-^{1}.K-^{1}) and a reduction over the western Sahel (MMM= -0.06 mm.d-^{1}.K-^{1}), which is consistent with the dipolar pattern as seen in previous generations of CMIP models (Monerie et al. 2017a; Almazroui et al. 2020; Monerie et al. 2021). The inter-model spread is the same for the Western and Central Sahel regions and therefore for the whole region (about 0.17 mm.d^{-1}.K^{-1}; see the statistics in the upper left corner of each panel in Fig.1). It is larger than the MMM especially for Western Sahel. There is a general agreement on the sign of the projected change for central Sahel but with a largely varying amplitude. However, there is no agreement on the sign of the projected change for Western Sahel and Sahel as a whole: one third of the models predict a reduction in precipitation and two thirds an increase. As we seek to establish links between the inter-model spread of Sahel precipitation change and changes elsewhere, we present first an overview of the MMM changes of global surface temperature and precipitation, as well as an outlook of the areas of greatest disagreement between the models regarding the change of these two variables.

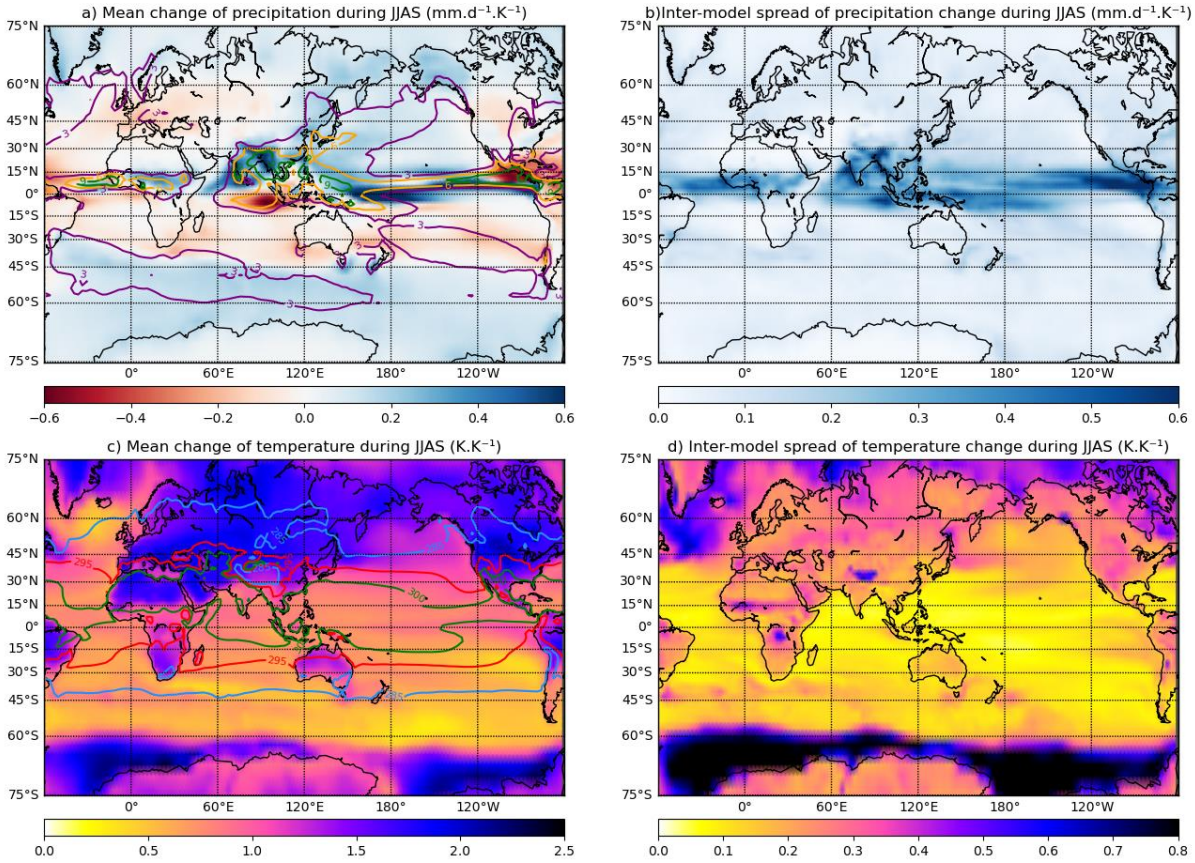

Fig. 2. JJAS MMM and inter-model spread of scaled precipitation (mm.d^{-1}.K^{-1}, top) and surface temperature (K.K^{-1}, bottom) changes computed for the 32 CMIP6 models. (a) MMM precipitation change, (b) inter-model spread of precipitation. (c) and (d) are the same as (a) and (b), respectively,

Accepted for publication in *Journal of Climate*. DOI 10.1175/JCLI-D-23-0162.1.

but for surface temperature. Contours in (a) are for JJAS precipitation present day (1979 to 2014) observed climatology (Global Precipitation Climatology Project (GPCP) monthly mean precipitation flux dataset (Adler et al. 2003), contour interval is 3 mm.day^{-1}) and in (c) for JJAS surface temperature present day climatology (ERA-Interim reanalysis (Dee et al. 2011), 285K blue, 295K red, 300K green contours). Temperature and precipitation changes are computed as the difference of climatological means between the end of the century (2064-2099) and the end of the historical period (1979-2014). See Section 2 for details.

Fig.2a displays the scaled JJAS precipitation changes over the 21st century in the SSP5-8.5 scenario, as defined in Section 2. As expected the main changes take place in the Tropics. Over the Sahel, we find a dipolar zonal rainfall pattern as in previous generations of CMIP (Roehrig et al. 2013; Monerie et al. 2013, 2021), with a decrease in rainfall over the western part of the Sahel and an intensification over the rest of the region in agreement with Fig.1. This rainfall zonal gradient over land is in fact part of a larger quadrupole rainfall pattern in the tropical Atlantic-WAM region (Fig.2a). Sahel rainfall presents one of the largest uncertainties in relative precipitation change and large disagreement regarding the sign of the change (Figs.1 and 2b; AR6). This large uncertainty is also a characteristic of the whole quadrupole rainfall pattern described above. The other monsoon regions around the world tend to show an increase of precipitation in the future, except Central America (Fig.2a). There is a large uncertainty about the magnitude of change over all monsoon regions, not only the Sahel, but the relative changes are the highest for the Sahel (Chen et al. 2020).

Overall, Fig.2a shows that the most important changes in precipitation over the ocean occur in the Pacific ITCZ, which shows both a strong intensification and an asymmetric double ITCZ structure. Fig.2a displays also a precipitation zonal dipole around the maritime continent, with an intensification of precipitation in the central and eastern Pacific and a decrease in precipitation in the southeastern Indian Ocean. This feature is consistent with the emergence of an Indian Ocean Dipole (IOD) mean state changes in the SSP5-8.5 scenario of CMIP6 (see Fig.8.6 in Cherchi et al. 2021). This Indo-Pacific dipole is also consistent with the evolution towards an El Niño-like mean SST state in the Indo-Pacific region in the SSP5-8.5 scenario (Fig.2c; see also Lian et al. 2019; Cherchi et al. 2021). There is also a strong inter-model spread across the Pacific, more pronounced in the eastern part of the basin (Fig.2b), which is also consistent with the large inter-model spread affecting the American monsoon in CMIP5 (Pascale et al. 2017).

Accepted for publication in *Journal of Climate*. DOI 10.1175/JCLI-D-23-0162.1.

In terms of scaled temperature change during boreal summer (Fig.2c), it is no surprise that the continents are warming more than the oceans in the Northern Hemisphere and vice versa for the Southern Hemisphere and also that lands in the Northern Hemisphere are warming more than in the southern one. Over land, the greatest uncertainties are found in the Himalayas, the Sahel and Central Africa (Fig.2d). There are, in particular, large uncertainties over the Sahara and Europe, which have both been pointed out as regions that may influence the Sahel monsoon (Cook and Vizy 2015; Biasutti 2019; Zhang and Li 2022). Uncertainties are less pronounced over the Asian monsoon regions, which is surprising given the uncertainties in precipitation described above, but may be explained by the fact that the temperature changes are mainly controlled by the precipitation changes in this region (Guilbert et al. 2023). Turning now to the SSTs (Fig.2c) and focusing first on the Tropics (see supplementary Fig.S1 for a zoom on the Tropics), one of the major robust changes over CMIP generations of models is that the mean state of the Pacific tends to be more El Niño-like, with a more pronounced warming in the east of the basin. The mean state of the Indian Ocean is more positive IOD-like, which is consistent with the strong coupling between the two oceanic basins (Lian et al. 2019; Cherchi et al. 2021). Large uncertainties regarding the amplitude of the eastern Pacific warming persist nonetheless (Fig. 2d), similarly to the historical period (Guilbert et al. 2023). At extratropical latitudes, ocean surface warming is maximum around the South pole and this warming is also greater than the one observed over the land of the Northern Hemisphere during boreal summer. Model uncertainties are also largest around the South Pole, where inter-model spread maxima are found, and, secondary, in the northern Atlantic subpolar gyre (Fig.2d). Overall, uncertainty is much stronger for the Southern Hemisphere and the North Atlantic than for the tropical SSTs, but the Southern Hemisphere is the most uncertain.

Given the large and global inter-model spread of surface temperature and precipitation changes, and the complex teleconnections linking the Sahel rainfall with the rest of the globe (Janicot et al. 2011; Martin et al. 2014; Giannini and Kaplan 2019; Nakanishi et al. 2021), we will track in the following section the main sources of inter-model spread of Sahel rainfall change on a global scale, by using a series of MCA analyses.

4. Sources of Sahel precipitation change uncertainties

a) *Global temperature and precipitation changes associated with Sahel rainfall*

Accepted for publication in *Journal of Climate*. DOI 10.1175/JCLI-D-23-0162.1.

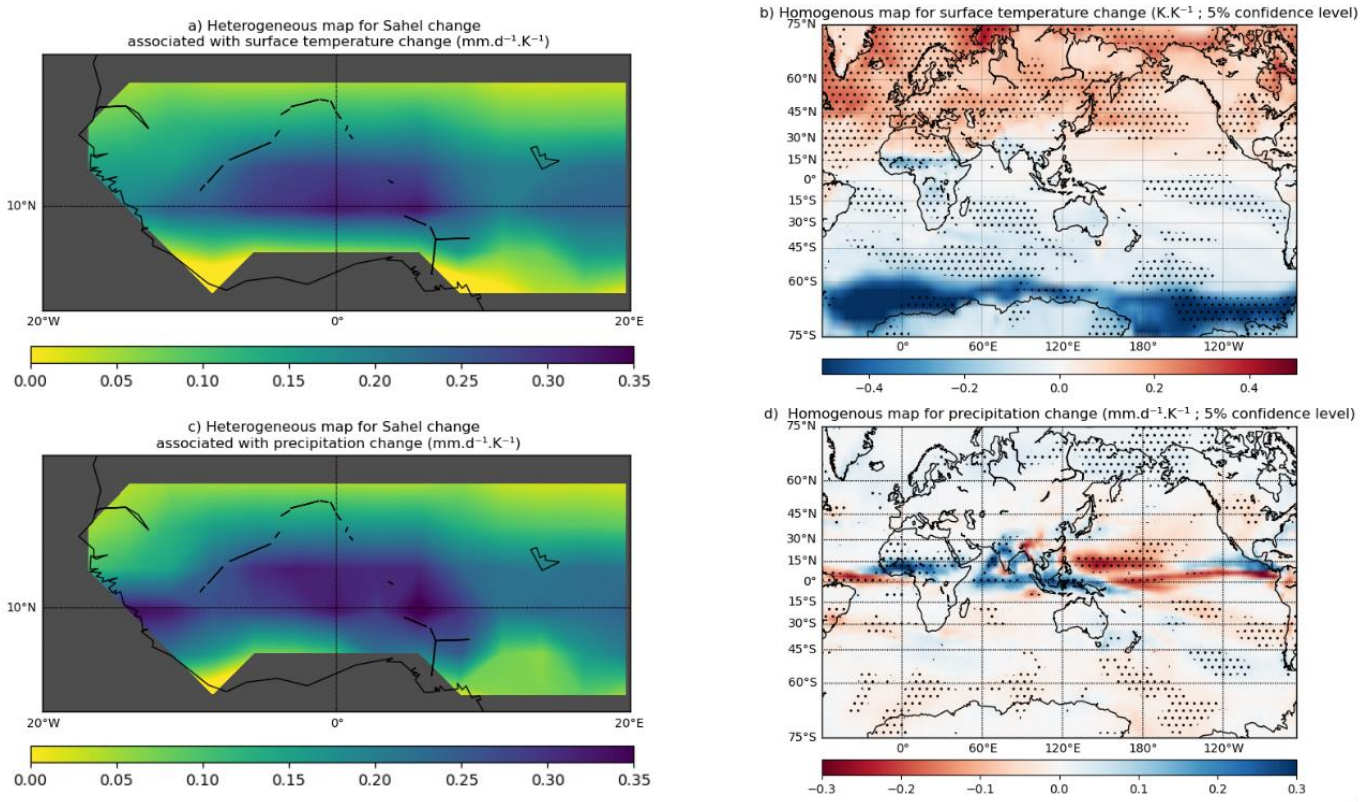

Fig. 3. Heterogeneous (a) and homogeneous (b) maps obtained from the MCA analysis performed between the scaled global surface temperature change (K.K^{-1}) of the 32 climate models and the scaled Sahel precipitation changes (mm.d^{-1}.K^{-1}) in the same 32 models. (c) and (d): same as (a) and (b) for the MCA between the scaled global precipitation change (mm.d^{-1}.K^{-1}) and the Sahel precipitation change (mm.d^{-1}.K^{-1}). Precipitation and temperature fields are scaled by global temperature change (see text and Section 2 for details). Homogeneous and heterogeneous maps show pointwise covariances between the grid-point model series and the respective standardized SV model series. The units on the maps are thus the same as the original field (mm.d^{-1}.K^{-1} for rainfall and K.K^{-1} for temperature). Dotted points indicate pointwise correlations significant at the 95% confidence level between the respective SV and grid-point model series using a Student test and 31 degrees of freedom (see Section 2).

We compute two MCAs, one between changes in precipitation over the extended Sahel region and changes in global surface temperature (Figs.3a,b), and the other one between changes in precipitation over the extended Sahel and global precipitation changes (Figs. 3c,d). It is important to note that the patterns derived from the MCAs are centered around the MMM of

Accepted for publication in *Journal of Climate*. DOI 10.1175/JCLI-D-23-0162.1.

the change for each of the variables (Fig.2a,c). So, whenever we refer to cooling/warming or drying/wettening, we must bear in mind that this is always with respect to the MMM change of the related variable.

First, in a preliminary MCA analysis, to assess the influence of internal variability on our MCA results, we recompute the two MCAs by considering all members available for each model (see Table.S1) and averaging them before computing the covariance matrix (see Fig.S3). The extreme similarity between Figures 3 and Fig.S3 shows that internal variability does not play an important role, as damping it further by considering multi-member averages has no impact on the relationships highlighted by the MCAs. This shows that the 35-years average is sufficient to dampen internal variability, which in any case plays only a minor role in the inter-model spread of precipitation change in the Sahel over the late 21st century according to Monerie et al. (2021).

Second, in order to assess the possible influence of the climate sensitivity of the models on the MCA results, we also performed the MCAs both with and without global temperature scaling (see Fig.S4 for the unscaled versions of the MCAs). The MCA patterns of precipitation change over the Sahel or globally are again robust (compare Fig.3.a,c,d and Fig.S4.a,c,d), as they remain unchanged whether the temperature scaling is applied or not. However, as global warming is a very strong signal and is an important amplifying factor of the inter-model spread of surface temperature (compare Fig.2 and Fig.S2), it influences the first temperature MCA pattern (Fig.3b and Fig.S4.b) even though it has no impact on the corresponding rainfall change in the Sahel, as we have just discussed (Figs.3a,c and Figs.S4a,c). This phenomenon is also well illustrated by the strong and significant relationship between the global warming series across the models and the SV series of unscaled temperature change (r=0.90), while the SV of unscaled Sahel rainfall change shows no significant relationship with this global temperature series (r=0.20, P-value>0.20). Thus, given that the climate sensitivity of each of the models can artificially blur the signal of interest for the Sahel, we have chosen to work with scaled quantities, as also done routinely in many previous studies (Kent et al. 2015; Li et al. 2017; Zhang and Li 2022). This allows to eliminate the effect of the large spread of equilibrium climate sensitivity in CMIP6 models (e.g., Meehl et al. 2020; Zelinka et al. 2020) as an additional source of inter-model difference. This amounts to an analysis of climate responses between models for the same level of warming.

Accepted for publication in *Journal of Climate*. DOI 10.1175/JCLI-D-23-0162.1.

We consequently focus only on the leading mode for each of the "scaled" MCAs, as they describe most of the covariability between the original fields (Table 2) and they explain much more inter-model spread of Sahel rainfall change than the second MCA mode (51% against 17%). The SCF and NC statistics, characterizing the strength of the coupling in the MCA (see Section 2 and Text. S1 for a detailed definition of these MCA statistics), are strong (see Table 2) and significant at the 1% level for the leading modes, which again corroborates the reliability of these modes.

The associated heterogeneous maps (see Section 2 and Text. S1) of rainfall changes over extended Sahel are similar in both MCA computations (Figs.3a,c). The spatial loadings are fairly homogeneous and positive, but with weaker values at the edges of the domain. Consistently, the correlations between the SV model series associated with the rainfall change patterns over the extended Sahel (Fig.3a and Fig.3c respectively), and precipitation averaged over the canonical Sahel are, respectively, 0.99 and 0.94.

Finally, the rainfall changes patterns from the MCAs (Figs.3a,c) are also very close to the first Empirical Orthogonal Function (EOF) mode of Sahel rainfall change (not shown): the leading modes from EOF and MCA are correlated with r=0.89 and the variance explained by these modes are again very close (51% for the first mode of EOF and 50% for both MCAs) despite that the MCA is designed to maximize the covariance between the two fields rather than the explained variances of the fields.

These results further motivate a detailed analysis of the covariability of these modes of inter-model spread of Sahel rainfall change with local and remote factors. The correlations between the SV series of the main modes of precipitation and temperature changes (Fig.3b and Fig.3d) and those of the Sahel precipitation change (Figs. 3a and 3c) highlight strong and similar statistical relationships within the two pairs of fields (0.89 and 0.80 respectively; see Table 2). This suggests first that projected precipitation and surface temperature inter-model spreads have relationships of rather equivalent strength with the inter-model spread of Sahel rainfall change and, second, the existence of regional or global ocean-atmosphere and/or land-atmosphere couplings that modulate the Sahel rainfall projections across the models. Consistently, there is a significant linear relationship between the leading SV model series of the main precipitation and temperature change patterns (Fig.3b and Fig.3d) associated with Sahel precipitation changes (r=0.70).

Accepted for publication in *Journal of Climate*. DOI 10.1175/JCLI-D-23-0162.1.

Fig.3b shows that associated with an intensification of Sahel rainfall, there is a strong global contrast between the Northern and Southern Hemispheres with an anomalous warming north of 15°N and an anomalous cooling south of 15°N during boreal summer. The southern cooling is particularly strong at high latitudes and its amplitude is greater than the northern warming at the same latitudes. This is consistent with Figure 2d, which also shows that the inter-model spread of scaled surface temperature is greatest at high southern latitudes and not in the Northern Hemisphere or North Atlantic during JJAS. Importantly, the pointwise correlations between temperature changes and the associated SV series (see Fig.3b) are also equally important in both hemispheres. This inter-hemispheric temperature gradient is superimposed on the global (uniform) warming simulated by all models, not shown here as it has been eliminated by the temperature scaling. In a global energetic framework of the ITCZ (Schneider et al. 2014; Byrne et al. 2018; Biasutti et al. 2018), such inter-hemispheric temperature gradient is associated with an inter-hemispheric radiative imbalance and a migration of the Hadley cell system and the associated ITCZ towards the warmer hemisphere. The lower branch of the Hadley circulation indeed transports moisture towards the warmer hemisphere, which is materialized by the migration of the ITCZ. It allows energy to be transported towards the cooler hemisphere along its reinforced upper branch to compensate for the energy imbalance. Fig.S5 corroborates the involvement of the lower branch of the Hadley cell by showing a well defined strengthening of subtropical highs and trade winds in all oceanic basins of the Southern Hemisphere. Note that the inter-hemispheric temperature and SLP gradients and the associated inter-hemispheric low-level atmospheric flow are particularly well defined in the Atlantic sector as expected. Moreover, the associated strengthening of the Southern Hemisphere trade winds is consistent with the significant cooling observed at the margins of subtropical highs in the Southern hemisphere in all three oceanic basins (Fig.3b).

In addition to this large-scale inter-hemispheric signature, there is a significant cooling over the eastern and central equatorial Pacific (Fig.3b) that modulates significantly the El-Niño like warming found in the MMM (Fig.2c, see also Lian et al. 2019, Fredriksen et al. 2020). This suggests that models with a less El Niño-like temperature change in the tropical Pacific tend to project an intensification of precipitation in the Sahel (Fig.3b). This is plausible given the strong negative correlation found in observations between El Niño-Southern Oscillation (ENSO) and rainfall in the Sahel on interannual time scales (Joly and Voldoire 2009; Janicot et al. 2011). In the observations and at interannual timescales, such SST anomalies exert an influence on the atmosphere by shifting the heat sources associated with deep convection, with

Accepted for publication in *Journal of Climate*. DOI 10.1175/JCLI-D-23-0162.1.

the upper tropospheric heating propagating through the Tropics in the form of Kelvin and Rossby waves (Trenberth et al. 1998; Shaman and Tziperman 2007; Joly and Voldoire 2009). Yet, it remains to be proven that similar mechanisms are at work for explaining a part of the inter-model spread of Sahel rainfall projections, and that they apply in the case of changes in the mean state of the equatorial Pacific rather than in ENSO variability (see below). Note that the anomalous cooling occurring in the southeastern tropical Pacific could be related to both the emergence of this La Niña-like pattern with respect to the MMM and the strengthening of the subtropical anticyclone discussed above (see Fig.S5), and therefore be related to both the near global inter-hemispheric gradient and the ENSO-like mean-state. This aspect is further detailed in Subsection 4b below.

From the rainfall perspective, Fig.3d shows a large rainfall modulation over the entire Sahel band. Along the western side of Africa, it extends in latitude up to 30°N. Along the equatorial Atlantic, Fig.3d displays a band of decreasing rainfall which could be associated with the increase in Sahel rainfall. In this case, it could be interpreted as a northeastward shift of the ITCZ, which would be partly consistent with the inter-hemispheric surface temperature and SLP patterns described above. Nevertheless, Fig.3d shows that this northward migration of the ITCZ is not found in other basins, suggesting that there are other important factors besides the inter-hemispheric temperature gradient. In connection with the MCA analysis we have conducted on global temperature changes (Fig.3b), a plausible candidate is the modulation of equatorial Pacific SSTs, which are known to exert a strong influence on tropical precipitation and could dominate over the inter-hemispheric temperature gradient in these regions. For example, Fig.3d shows that the Arabian sea and India also experience enhanced rainfall for models projecting a wet Sahel. This feature is consistent with the role of central Pacific SSTs if we assume that the mechanisms involved in interannual variability also apply to changes, which remains to be proven (see Section 5b). Indeed, the Indian and African monsoons covary under the influence of ENSO in the observations (Madhavan et al. 2022). Accordingly, the Pacific Ocean presents a strong signal of precipitation change, with stronger than average precipitation over the Maritime Continent and the Indian region, but a weaker precipitation over the NWP monsoon area, all of which are consistent with the variability of Indo-Pacific precipitation during La Niña events (Timmermann et al. 2018; Tao et al. 2022). However, even if the intensification of precipitation over the western part of the Indo-Pacific region is consistent with an enhanced zonal circulation, the most significant signal is the drying on the

Accepted for publication in *Journal of Climate*. DOI 10.1175/JCLI-D-23-0162.1.

northwestern part of the Pacific Ocean, which is under the influence of the NWP monsoon system. Therefore, rainfall changes in the Indo-Pacific region could also be related to a westward shift in the zonal circulation rather than an intensification alone. Finally, Fig. 3d shows a drying in the vicinity of the Southern Hemisphere subtropical highs in each of the three ocean basins, which is consistent with a strengthening of the Hadley cells and supports the importance of the inter-hemispheric temperature gradient described above.

To conclude, the MCA analyses highlight an increased inter-hemispheric gradient and an ENSO-like signature as important factors associated with the differential response of Sahel rainfall in the CMIP6 projections.

	Explained variances of Extended Sahel rainfall change by the first leading mode in each MCA	SCF	NC	Correlations between the first SVs of rainfall change over extended Sahel and Sahel averaged precipitation change	Correlation between first SV of global change and first SV of rainfall change over Sahel	Correlation between the first SVs of global precipitation and surface temperature change from the two MCAs (Figs.3bd)	Correlation between the first SVs of rainfall change over the Extended Sahel from the two MCAs (Figs.3ac)
MCA: global rainfall change with Sahel rainfall change	51 %	68 %	22 %	0,93	0,89	0,70	0,99

Accepted for publication in *Journal of Climate*. DOI 10.1175/JCLI-D-23-0162.1.

MCA: global temperature change with Sahel rainfall change	49 %	79 %	25 %	0,95	0,80		

TABLE 2. Statistics associated with the MCAs between global scaled surface temperature or precipitation changes with Sahel rainfall change shown in Fig.3. All correlations in the last four columns are significant at the 99% confidence level considering each model independent. See text and Text.S1 in the supplemental material for more details on the SCF and NC statistics.

b) *Performance of averaged temperature indices in explaining Sahel rainfall change*

Accepted for publication in *Journal of Climate*. DOI 10.1175/JCLI-D-23-0162.1.

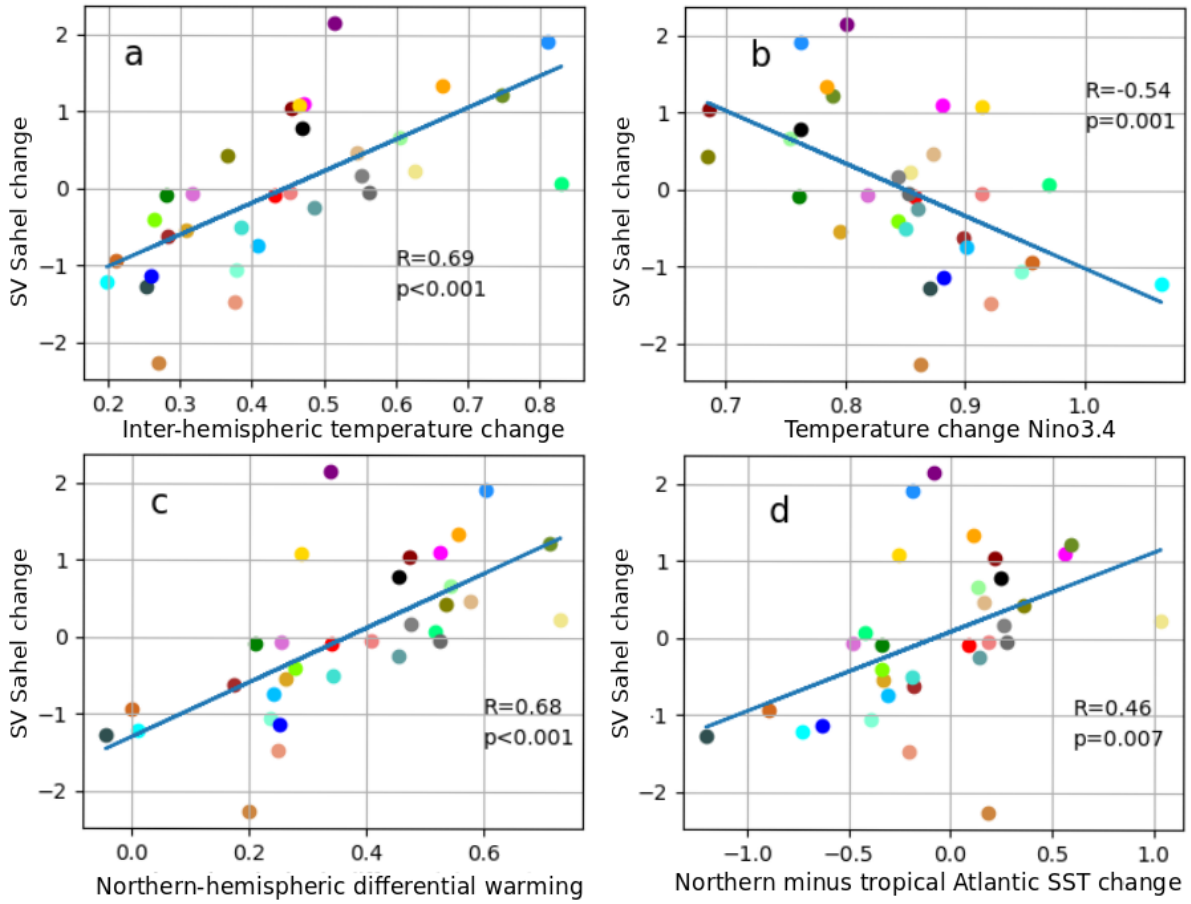

Fig. 4. Scatterplots of SV Sahel change (mm.d^{-1}.K^{-1}, from Fig.3a), respectively, with (a) inter-hemispheric temperature change (K.K^{-1}), (b) Niño3.4 temperature change (K.K^{-1}), (c) Northern-hemispheric SST differential warming (K.K^{-1}), (d) northern minus tropical Atlantic SST change (K.K^{-1}). The definition of each index can be found in Section 2 and Table 1. All model series are scaled by the global temperature change in each model. The correlation and its associated P-value for each pair of model series are indicated in each panel.

In view of the consistent results between the two MCAs, we choose to focus on selected key temperature indices representing well defined modes of variability or physical processes to explain the inter-model spread of Sahel precipitation change. The inter-hemispheric temperature gradient index has a strong correlation with the Sahel rainfall change spread (Fig.4a), stronger than the Niño3.4 index (Fig.4b), both being significant at the 99% significance level. Note that if we extend the regression line in Fig.4a to a zero change in the

Accepted for publication in *Journal of Climate*. DOI 10.1175/JCLI-D-23-0162.1.

inter-hemispheric temperature gradient, i.e., uniform warming, this relationship predicts a drier Sahel, which is consistent with the results of Chou and Neelin (2004), Held et al. (2005) or Gaetani et al. (2017) describing a stabilization of the tropical troposphere, and also with the dry air intrusions from the Sahara due the uneven atmospheric boundary layer moisture increase between convective and non convective regions, known as the upped-ante mechanism. Other indices, mostly inspired from previous studies (defined in Table 1), such as the Northern-hemispheric differential warming (Park et al. 2015) or differential warming between north and tropical Atlantic SSTs (Zhang and Li 2022) are also displayed, respectively, in Figs.4c and 4d. The differential warming between north and tropical Atlantic SSTs show consistent, but weaker correlation with the inter-model spread of Sahel precipitation change, whereas the index derived by Park et al. (2015) yields a correlation almost equal to the inter-hemispheric gradient index defined here.

Fig.4b confirms that the inter-model spread of Niño3.4 SST change is also significantly correlated with the inter-model spread of Sahel precipitation change. Interestingly, the inter-hemispheric temperature gradient is not significantly correlated with temperature change over Niño3.4 ($r=-0.25$, P-value=0.17), unlike both the Northern Hemisphere differential warming and the northern minus tropical Atlantic SST gradient (their correlations with Niño3.4 are, respectively, $r=-0.49$ (P-value<0.01) and $r=-0.42$ (P-value=0.02). This supports the choice of the inter-hemispheric temperature gradient and Niño3.4 SST as key indices to explain the Sahel rainfall change in the rest of the study. Furthermore, they are associated with well-defined modes of variability which are both known to be important for Sahel variability at interannual and/or decadal or centennial timescales (Biasutti et al. 2008; Joly and Voldoire 2009; Biasutti et al. 2018). This makes them both plausible candidates from the point of view of physical processes in addition to their statistical relevance for explaining the inter-model spread of Sahel rainfall projections.

In order to check for the existence of other potential drivers, we compute regression analyses of the SV of the Sahel precipitation change with surface temperature change after removing the effect of the inter-hemispheric temperature gradient index alone (top, Fig. S6) and of the effect of both the inter-hemispheric temperature gradient and Niño3.4 indices (bottom, Fig. S6). The results show that when we remove the linear contributions of both indices, there is almost no significant correlation left over the globe between surface temperature changes and

Accepted for publication in *Journal of Climate*. DOI 10.1175/JCLI-D-23-0162.1.

Sahel rainfall changes, except over the Sahel itself (Fig.S6b). The inter-hemispheric temperature gradient alone is however not sufficient to remove all the signal with the temperature changes, especially in the Pacific and at high latitudes of both hemispheres (Fig. S6a).

5. Mechanisms of future Sahel rainfall uncertainties

a) Inter-hemispheric gradient change and Sahel rainfall

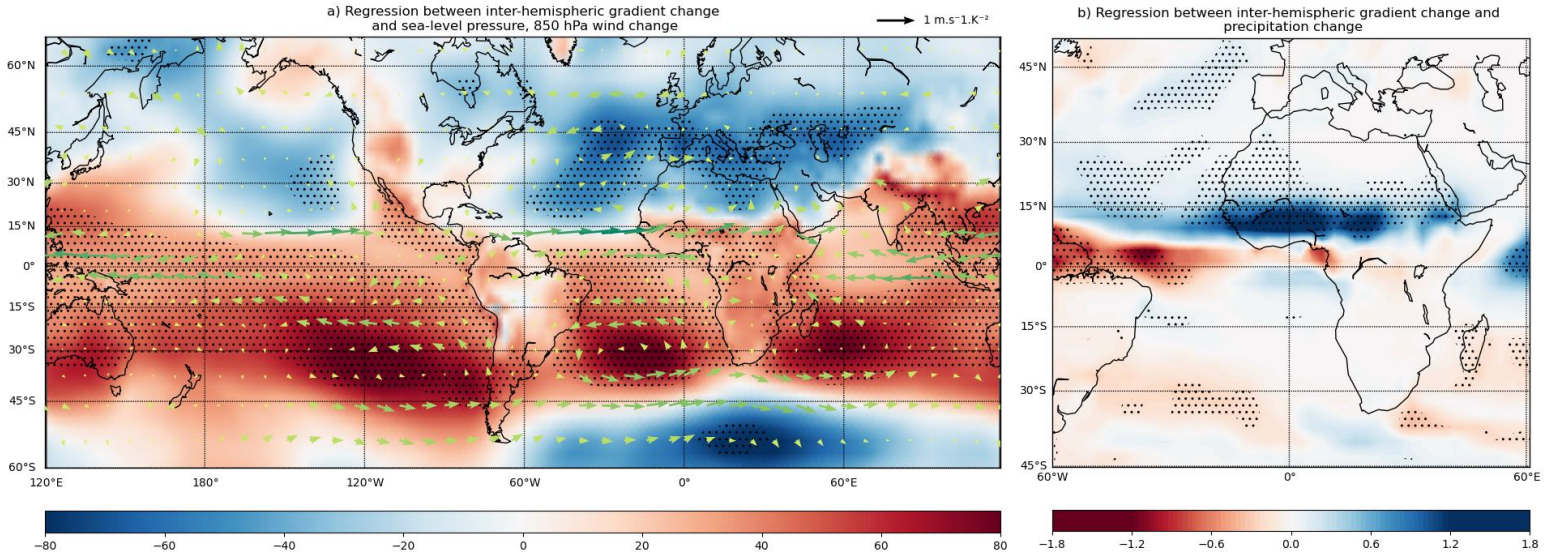

Fig. 5. Inter-model regressions against the inter-hemispheric temperature gradient change of (a): changes in SLP (color shaded, $Pa.K^{-2}$) and wind at 850 hPa (vectors, $m.s^{-1}.K^{-2}$); (b) precipitation change (color shaded : 0,1 $mm.d^{-1}.K^{-2}$). The colors of the arrows vary from green to yellow according to the intensity of the wind speed for readability. On panel (a), only 1 vector out of 3 is shown also for readability and dotted points indicate grid-points where the regression with sea-level pressure change is significant at the 95% confidence level. On panel (b), dotted points indicate grid-points where the regression with precipitation change is significant at the 95% confidence level.

Figure 5a shows that the models with an enhanced inter-hemispheric gradient in the future with respect to the MMM tend to produce an intensification of the subtropical highs in the Southern

Accepted for publication in *Journal of Climate*. DOI 10.1175/JCLI-D-23-0162.1.

Hemisphere and a reduction of those in the Northern Hemisphere in all oceanic basins as compared to the MMM. Consistently, the trade-winds in the south subtropics and the eastward low-level anomalous flow at about 15°N towards the West African, Indian and American monsoons regions are both stronger when the inter-hemispheric temperature gradient is enhanced. Note that these low-level wind, temperature and SLP gradients between the two hemispheres are reminiscent of the positive wind-evaporation-SST feedback linking the SST gradient and the cross-gradient flow in the Tropics at the interannual and decadal time scales (Chang et al. 1997; Chiang and Vimont 2004). This suggests that local coupled ocean-atmosphere interactions may also sustain this wind regime changes in both the Pacific and Atlantic basins.

These patterns of SLP and low-level wind changes are broadly similar to those associated with the first leading MCA mode of Sahel rainfall illustrated in Fig.S5, especially in the Southern Hemisphere. These similarities are further confirmed by the associated precipitation change (Fig. 5b), which depicts a northward shift of the ITCZ in the Atlantic sector, with a homogeneous intensification of precipitation over the Sahel and a decrease along the equator. An additional mechanism that may link an anomalously strong inter-hemispheric gradient change to enhanced precipitation change over the Sahel is the intensification of the West African Westerly Jet (WAWJ), which corresponds to the low-level winds around 10°N coming from the Atlantic and penetrating the African continent (Grodsky et al. 2003). Indeed, an enhanced WAWJ (Fig.5a) is linked to an increase in wind convergence and rainfall over the Sahel (Pu and Cook 2010). This is in agreement with previous studies such as Park et al. (2015) or Zhang and Li (2022), which point, respectively, to an amplification of low pressure over the Sahara or over Western Europe as the origin of these westerly wind anomalies. These regions are also highlighted in Fig.5a, but we emphasize here that the northward migration of the ITCZ could be also a key factor in the intensification of the WAWJ. Indeed, when the Atlantic ITCZ is shifted northwards, the southerly winds are stronger, which reinforces the eastward acceleration by the Coriolis force as they cross the Equator and reach the west coast of Africa, consequently reinforcing the WAWJ (Pu and Cook 2012).

Some differences between the SLP and wind anomalous patterns in the Northern Hemisphere in Fig.S5 and those associated with the globally enhanced meridional temperature gradient in Fig.5a are nevertheless noteworthy. Although both figures show high-pressure anomalies over the NWP, as well as the low-pressure anomalies over North Africa and Europe, these are more pronounced in Fig.S5 than in Fig.5a, as can be seen from the loss of significance over certain

Accepted for publication in *Journal of Climate*. DOI 10.1175/JCLI-D-23-0162.1.

parts of these regions. This suggests that other mechanisms are at work to complete the picture, notably from the influence of the equatorial Pacific SSTs that we suggested earlier.

b) Teleconnection between Niño3.4 *and Sahel rainfall*

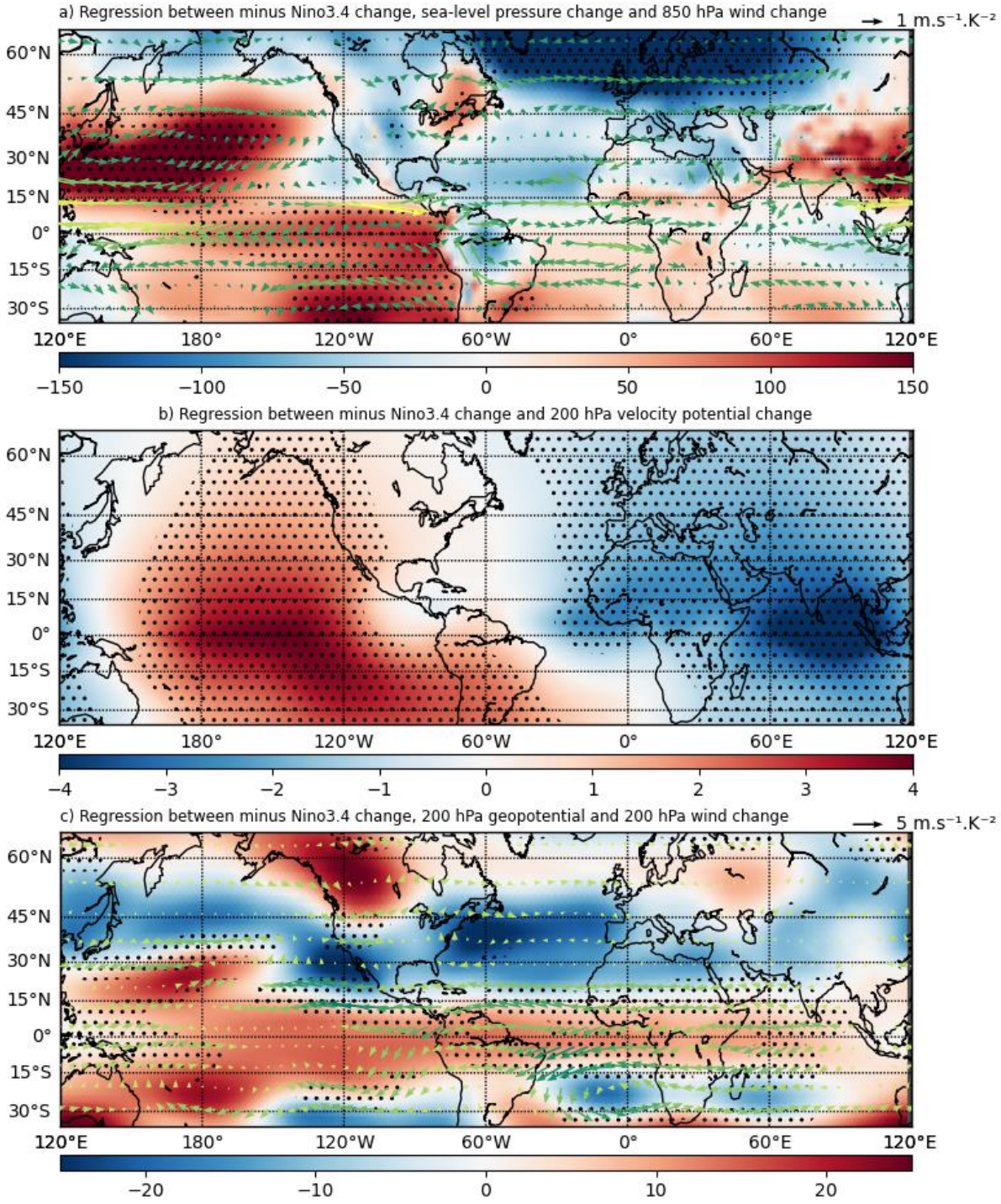

Accepted for publication in *Journal of Climate*. DOI 10.1175/JCLI-D-23-0162.1.

Fig. 6. Inter-model regressions against minus Niño3.4 temperature change of (a): SLP changes (color shaded, $Pa.K^{-1}$) and 850 hPa winds (vectors); (b) change of velocity potential at 200 hPa (color shaded, $x10^6$ $m^2.s^{-1}.K^{-2}$); (c) 200 hPa geopotential change (color shaded : $m^2.s^{-2}.K^{-2}$) and winds (vectors). "Minus Nino3.4" refers to the fact that we have taken the opposite of Nino3.4 in order to have a positive modulation of rainfall over the Sahel as in the MCA patterns of Fig. 3a and c.

In order to facilitate the comparison with the MCA results which display an intensification of Sahel rainfall (Fig.3ac), Figs. 6-8 show regressions with the opposite (minus) of the Niño3.4 index, thus featuring anomalous La Niña patterns with respect to the MMM. Note that this is an approximation within the linear framework of our study, as the (observed) El Niño/La Niña patterns are not simply opposite to each other, as we imply here (Su et al. 2010).

In the Tropics, a classic mechanism for remote large-scale teleconnections at interannual timescales arises from the fact that ENSO is associated with an eastward migration of the Indo-Pacific warm pool causing the Walker circulation to shift zonally (Trenberth et al. 1998; Joly and Voldoire 2009; Roy et al. 2019). The hypothesis that similar mechanisms are at work here for explaining a part of the inter-model spread of Sahel rainfall change is suggested by Fig.6. This is firstly seen via the surface variables changes associated with the inter-model changes in the (minus) Niño3.4 index shown in Fig.6a. Models with a La Niña-like change in the equatorial Pacific with respect to the MMM show a stronger and significant intensification of the subtropical anticyclone in the southeast Pacific and of the pressure gradient along the Equator, resulting in an intensification of the trade winds from 30°S to 5°N. To the west of the basin, there are also strong positive pressure anomalies around 30°N, which lead to strong anticyclonic circulation anomalies corresponding to a drastic weakening of the NWP monsoon during boreal summer. Taken together, these features strongly enhance wind convergence from the Pacific towards the Maritime Continent and the Indian Ocean, especially along the Equator, but also over South Asia as shown in Fig.7. Coupled with the westerly low-level wind anomalies over the Atlantic Ocean and Africa between 0° and 15°N, there is a consistent positive and significant precipitation anomaly over the African-Indian region (Fig.7). This illustrates a zonal shift of convection in the Indo-Pacific sector which is very similar to what is observed traditionally during developing La Niña events, with a weak NWP monsoon, and conversely during El Niños (Wang et al. 2001; Chou et al. 2003; Crétat et al. 2017).

Accepted for publication in *Journal of Climate*. DOI 10.1175/JCLI-D-23-0162.1.

Fig.6b further illustrates the pronounced shift of the Walker circulation from the perspective of the upper troposphere. It shows stronger than average velocity potential changes at 200hPa over the Pacific Ocean which correspond to anomalous convergence above the Pacific Ocean and, thus, a weaker convection for anomalous La Niña-like changes with respect to the MMM. Conversely, weaker than average changes of the velocity potential extending from the Indian Ocean to western Africa correspond to increased upper-level divergence associated with heavier rainfall over the Sahel and Indian sector (Fig.7). Therefore, through interactions with the large-scale circulation, a change in SST toward a less El Niño-like mean state in the Pacific Ocean in a particular model (see Supplementary Fig.S7, Lian et al. 2019) tends to produce amplified rainfall over the Sahel in this model compared to the MMM. This large-scale mechanism is broadly consistent with the rainfall changes observed in Fig.3d, which shows increased rainfall from West Africa to the Maritime Continent, and a decrease over the Pacific Ocean.

This link between Pacific mean state change and Sahel rainfall could also occur through the modulations of upper tropospheric jets and meridional tropospheric temperature gradient in the African-Asian sector during boreal summer (Sathiyamoorthy 2005; Shaman and Tziperman 2007; Nicholson 2009; Whittleston et al. 2017). Fig.6c shows that a La Niña-like SST change with respect to the MMM tends to produce easterly wind anomalies at 200 hPa from 120E to 90E which are symmetric about the Equator. This corresponds to a strong enhancement and a greater westward extent of the TEJ located between 5°N and 10°N. Such conditions are favorable to enhanced Sahel rainfall as an enhanced TEJ promotes uplift and upper-level divergence (Sathiyamoorthy 2005; Nicholson 2009, 2013; Whittleston et al. 2017). Furthermore, it is known that an increase of the vertical shear of the summer mean flow may be a primary factor leading to the northward propagation of the intra-seasonal convection and the rainfall band (Jiang et al. 2004; Sathiyamoorthy 2005; Whittleston et al. 2017; Bickle et al. 2021). The symmetry of 200 hPa dynamical features with respect to the equator first suggests that these upper-level zonal wind anomalies may be caused by the eastward propagation of a Kelvin wave from the equatorial Pacific (Joly and Voldoire 2009). Consistent with this view, Fig.6c shows 200 hPa geopotential anomalies extending along the Equator from the equatorial Pacific to Africa, reminiscent of a Kelvin wave signature from a Matsuno-Gill type response (Gill 1980). However, these equatorial 200 hPa geopotential anomalies are not statistically significant. Furthermore, the Kelvin wave response is centered at the Equator and decreases

Accepted for publication in *Journal of Climate*. DOI 10.1175/JCLI-D-23-0162.1.

rapidly away from the Equator while the TEJ position is at 10-15°N. Therefore the Kelvin wave response does not seem to be sufficient to explain the TEJ anomalies on their own. Nonetheless, Fig.6 also suggests additional pathways which may explain how models showing a more La Niña-like mean state than the MMM may also simulate an enhanced TEJ and thus WAM. First, the 200 hPa geopotential anomalies (Fig.6c) associated with the minus Niño3.4 index exhibit anomalous maxima and minima centers over the North Pacific, North America and the North Atlantic, which appear to be consistent with the extratropical teleconnections mediated through Rossby wave propagation associated with ENSO in observations and models (Trenberth et al. 1998; García-Serrano et al. 2017). The positive 200 hPa geopotential anomalies above the North Atlantic produced by this extratropical wave train can modulate tropospheric properties above 15°N and, thus, the TEJ. Indeed, although 200 hPa geopotential changes around the Sahel related to the minus Niño3.4 index are not individually significantly, the geopotential thickness (between 200 and 850 hPa) gradient around the Sahel (see Section 2 and Table 1 for details) is significantly linked to the (minus) Niño3.4 index ($r=0.46$, $p<0.01$). This is also consistent with the fact that the main effect of Pacific SST changes during boreal summer is to modulate the meridional tropospheric gradient in the African-Asian sector as a response to associated westward propagating Rossby waves (Shaman and Tziperman 2007). Thus, via the thermal wind relationship, this tropospheric thickness gradient is also strongly related to the vertical wind shear over the Sahel, itself largely driven by the TEJ and the Pacific mean state. Therefore, a change of the Pacific mean state could be linked to a change in the TEJ via both tropical and extratropical pathways, resulting in modulation of Sahel rainfall by promoting or inhibiting deep convection.

Accepted for publication in *Journal of Climate*. DOI 10.1175/JCLI-D-23-0162.1.

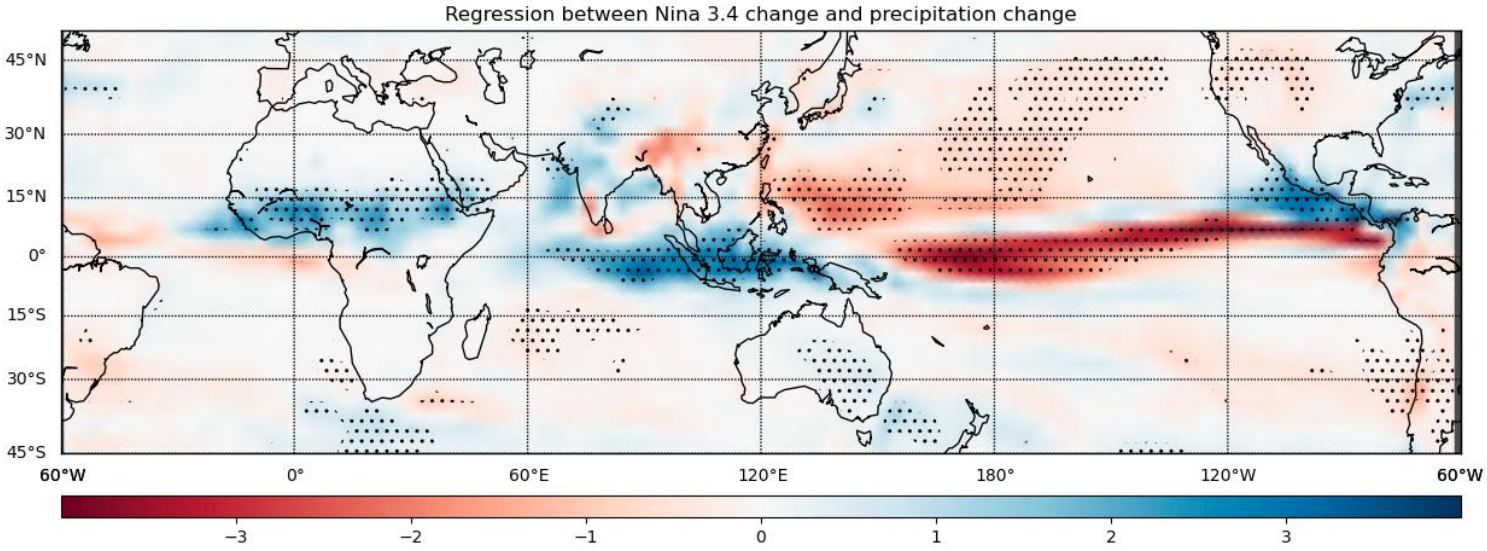

Fig.7. Inter-model regression of precipitation change against minus Niño3.4 temperature change ($mm.d^{-1}.K^{-2}$)

c) Respective contributions of the inter-hemispheric gradient and Niño3.4 index to the inter-model spread of Sahel rainfall

The sources of uncertainty in Sahel precipitation that we have highlighted have so far been considered as independent to first order. Nevertheless, although not statistically significant, there is still a correlation between the two indices (r=-0.25, P-value=0.17) which have thus some cross effects. In order to quantify their global and collective contributions to the inter-model spread of Sahel rainfall, we first use a bilinear regression model with these two indices. The parameters of the bilinear model is computed using a least squares optimization which aims to minimize the sum of the squared differences between the target variable and the values predicted by the model with the two explanatory variables. In our case, the target variable is the SV of precipitation change in the Sahel, and the predictor variables are the changes in the inter-hemispheric temperature gradient and Nino3.4 SST. This simple bilinear model explains 62% of the inter-model spread of the SV of Sahel precipitation change (R^2=0.62, r=0.79), which is very close to the inter-model spread explained by the temperature pattern from the MCA

Accepted for publication in *Journal of Climate*. DOI 10.1175/JCLI-D-23-0162.1.

(R^2=0.64, r=0.80). Similar results are obtained when we consider the precipitation change average over the Sahel canonical domain (not shown). In other words, the two indices taken together explain a very similar amount of future Sahel rainfall change spread as the first MCA mode shown in Fig.3.

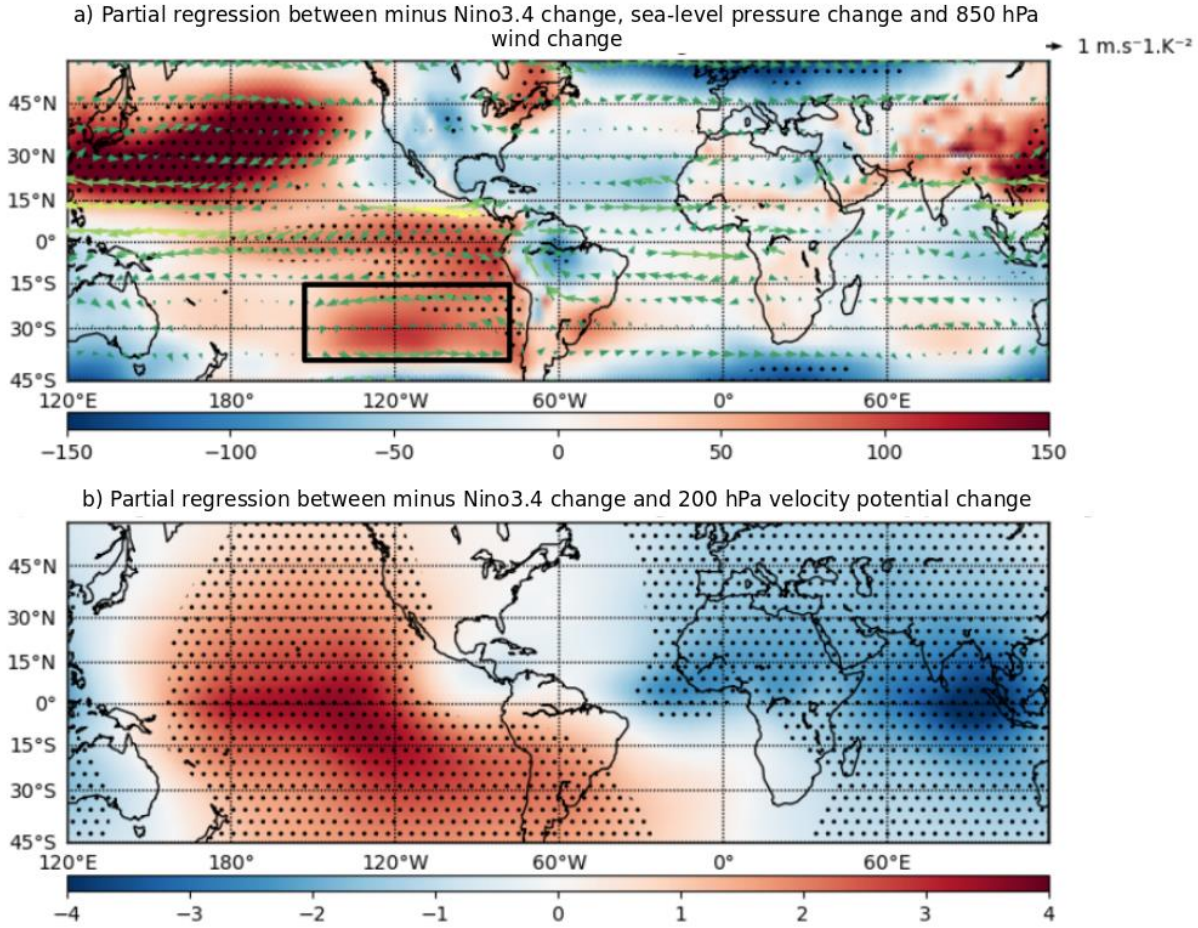

Fig. 8. Partial regression between minus Niño3.4 index change with changes in (a) SLP and 850 hPa winds -; (b) 200 hPa velocity potential; excluding in all variables their linear dependance to the inter-hemispheric temperature change (see Section 2 for details). Dotted points indicate significant correlations at the 95% confidence level. The black square emphasizes the area that lost intensity and significance compared to Fig.6a.

Next, to estimate the individual contribution of the interhemispheric temperature gradient and the equatorial Pacific SST change to the uncertainty, we use partial regressions that allow to

Accepted for publication in *Journal of Climate*. DOI 10.1175/JCLI-D-23-0162.1.

isolate the effect of one index by removing the linear contribution of the other. The contributions of the inter-hemispheric gradient and Nino3.4, assuming the other factor is held constant, are estimated to be 34% and 16%, respectively. What remains of the 62% of the spread explained by the bilinear model, i.e. 12%, corresponds to the role of the interactions between the two indices. This redundancy is not small and therefore can't be overlooked. This is illustrated first by the comparison between Figs.8a and 6a, which shows that the strength of the subtropical anticyclone in the South-East Pacific Ocean (see the black box in Fig.8a) decreases considerably and loses significance when considering the 'pure' influence of the minus Niño3.4 index after the removal of the linear contribution of the inter-hemispheric gradient. Similarly, in the upper-troposphere (compared Fig.8b with Fig.6b): the anomalous pattern is the same, but the amplitude of the velocity potential anomalies are smaller when the contribution from the inter-hemispheric temperature gradient is removed.

Finally, to estimate the individual contributions from the two indices, which correspond to the "pure" contribution of each of them, plus a part of the interactions, we use three different attribution methods as described in Section 2. As shown in Table 3, the three methods give very similar results, which gives confidence in the robustness of the results. By averaging the results of the three methods, we find that 40% of the inter-model spread of precipitation change over the Sahel is explained by the inter-hemispheric gradient and 22% by the SST Pacific mean state. This corresponds, on average over the methods, to an equal distribution of the 12% of the interactions to each of the two indices. Thus, we confirm, as previously supposed, that the inter-hemispheric gradient is the main source of uncertainty, and that the the tropical Pacific mean state is a secondary, but critical, source of uncertainty for Sahel rainfall projection and its spatial modulation, which may also positively interact with the inter-hemispheric gradient. Our results are consistent with Monerie et al. (2021) who shows that the fast response of the Sahel precipitation is associated with a reinforced inter-hemispheric gradient of temperature and explains most of the uncertainty. Moreover, our estimate of the inter-model spread of the change in precipitation in the Sahel explained by Nino3.4 is also consistent with the part explained by the slow response of the Sahel precipitation in Monerie et al (2021), which may be partly associated with the equatorial Pacific according to the same study.

Accepted for publication in *Journal of Climate*. DOI 10.1175/JCLI-D-23-0162.1.

	Dominance analysis	*Permutation Feature Importance*	*Random forest attribution*
Niño3.4 estimated contribution	*23%*	*22%*	*20%*
Inter-hemispheric gradient estimated contribution	*39%*	*40%*	*42%*

TABLE 3. Relative contributions of Niño3.4 and inter-hemispheric gradient to the inter-model spread of the SV of Sahel rainfall change, estimated with three different attribution methods (see Section 2 for details).

6. Conclusions and discussion

The response of Sahel monsoon rainfall to global warming suffers from large uncertainties which have not decreased from CMIP3 to CMIP6 (Monerie et al. 2020a; Zhang and Li 2022), and the origins of this inter-model spread are not yet well understood. In this study, we analyze 32 coupled models from CMIP6 under a high emission scenario (SSP5-8.5) in order to revisit the sources of Sahel rainfall change uncertainties at the end of the 21st century.

Our results first confirm that Sahel rainfall change in CMIP6 still suffers from large uncertainties with one third of the models projecting a decrease in precipitation and two thirds an intensification. The MMM change of Sahel precipitation exhibits a dipolar pattern with an increase over the central Sahel and a decrease in the western Sahel as in previous CMIP generations (Monerie et al. 2017b; Almazroui et al. 2020), but this zonal contrast is not apparent in the inter-model spread, which is fairly homogeneous over the Sahel. This suggests that mechanisms responsible for this spread induce primarily zonally homogeneous changes, which will be confirmed later by the predominant role of the inter-hemispheric temperature gradient in the model's responses.

Accepted for publication in *Journal of Climate*. DOI 10.1175/JCLI-D-23-0162.1.

On a broader scale, CMIP6 models also present large uncertainties regarding precipitation and temperature changes in different regions, which may be associated with these Sahel rainfall uncertainties. The greatest inter-model spread in surface temperature is found at high latitudes, with a maximum around the South Pole, which also concentrates the greatest warming, and then in the North Atlantic subpolar gyre. While many studies have focused on the role of the Northern Hemisphere as a source of uncertainty for Sahel precipitation (Park et al. 2015; Monerie et al. 2020b; Bellomo et al. 2021; Zhang and Li 2022), a global approach seems necessary in view of these results. Alternatively, the Sahara and Eurasia also show a large inter-model spread of surface temperature changes. This is consistent with previous studies which suggest that they are potential drivers of the change of the Sahel monsoon under global warming across the models (Park et al. 2015; Zhang and Li 2022). Finally, CMIP6 models present significant uncertainties regarding precipitation and SST changes in the Tropics, notably over the Pacific Ocean. Indeed, although the models agree on a rather El-Niño-like warming in the equatorial Pacific in the SSP5-8.5 scenario, the magnitude of this change is also highly uncertain (Lian et al. 2019; Fredriksen et al. 2020). Given the strong teleconnection linking equatorial Pacific SSTs to the Sahel (Trenberth et al. 1998; Biasutti et al. 2008; Joly and Voldoire 2009), they are also a plausible candidate, albeit overlooked in the literature, to explain the inter-model spread of Sahel monsoon change. Following this overview of the changes and related uncertainties from the models in CMIP6, we answered the three questions that had been raised in the introduction concerning the inter-model spread of Sahel rainfall change :

1. Can we revisit and improve the factors explaining the projected Sahel rainfall uncertainties from an objective analysis of the projected changes at the ocean-atmosphere-land surface ?

   The MCA analyses show that changes in global precipitation and surface temperature are both associated with the change in Sahel precipitation. However, this modulation is more important in the central Sahel than at the eastern and western edges of the region. The close correspondence between the two MCAs demonstrate that coupled ocean-atmosphere and land-atmosphere changes are linked to the uncertainties in Sahel rainfall change. In order to compare our results with previous studies, we choose to focus on the impact of surface temperature changes which highlight two major sources

Accepted for publication in *Journal of Climate*. DOI 10.1175/JCLI-D-23-0162.1.

of uncertainties: an inter-hemispheric temperature gradient and the equatorial Pacific mean-state represented here by a Niño3.4 index. While previous studies have mainly focused on the Atlantic Ocean and the Northern Hemisphere (Biasutti et al, 2008; Park et al, 2015; Zhang and Li, 2022), our study suggest an alternative choice overlooked for 21st century projections, the inter-hemispheric temperature gradient during boreal summer, which is a known source of Sahel monsoon variability (Biasutti et al, 2013) and more generally for latitudinal shifts of the ITCZ if we interpret it as a proxy for the inter-hemispheric radiative imbalance (Voigt et al. 2014; Haywood et al. 2016; Hawcroft et al. 2017). As for the equatorial Pacific SST, a few studies have used their interannual variability (e.g., ENSO) as a surrogate to evaluate the trend of tropical and Sahel precipitations in the 21st century across the models (Douville et al., 2006; Biasutti et al., 2008). However, these studies did not directly address the issues of uncertainty in the forced monsoon response across models and their links to the uncertainties in the Pacific mean-state.To the best of our knowledge, only Monerie et al. (2021) suggested a role for equatorial Pacific SSTs in explaining the inter-model spread of Sahel monsoon changes.

In addition to being strongly correlated with Sahel precipitation change, these two indices are not significantly correlated with each other, which allows us to consider them as two independent sources of uncertainty in a first statistical approximation. It should be remembered that MCAs can be used to demonstrate relationships, but not causality. Causality arises from the physical mechanisms described below.

2. By what physical processes are these factors related to Sahel rainfall?

The major processes which link the inter-model spread of Sahel rainfall change to the two factors mentioned below are summarized in Fig.9.

Accepted for publication in *Journal of Climate*. DOI 10.1175/JCLI-D-23-0162.1.

a) The inter-hemispheric temperature gradient impacts Sahel rainfall change by modulating the position of the ITCZ. Based on the energetic framework and the assumption that this gradient is a good proxy for the radiative imbalance between the two hemispheres during boreal summer (Schneider et al. 2014; Byrne et al. 2018), an increased inter-hemispheric gradient results in a northward shift of the ITCZ and enhanced rainfall over the Sahel. Our results highlight that the Southern and Northern Hemispheres are both essential in this process (Voigt et al. 2014; Haywood et al. 2016; Hawcroft et al. 2017). A complementary regional mechanism is that the northward migration of the ITCZ intensifies the WAWJ, leading also to an intensification of monsoon rains (Pu and Cook 2012). The associated rainfall modulation is homogeneous over the Sahel, and the spatial modulation of the MCA mode of Sahelian rainfall change (Fig.3ac) is provided by changes in the mean state of the equatorial Pacific.

b) The change in the equatorial Pacific mean-state has an impact firstly via the large-scale overturning zonal circulation in the Tropics. Indeed, for the models exhibiting a less El-Niño-like anomalous SST change, the Walker circulation is strongly shifted westward compared to the MMM (which is El-Niño-like), creating anomalous divergence in the upper-troposphere that extends over the Sahel and promotes local convection. The situation is reversed for more El-Niño-like models. Secondly, by modulating the latent heat release, SST changes in the equatorial Pacific modulate both the intensity and position of tropospheric warming and, subsequently, generate tropical Kelvin and extra-tropical Rossby waves that modify the meridional tropospheric temperature gradient around the Sahel (Shaman and Tziperman 2007). This ultimately leads to changes in the low- and upper-level zonal circulation over the Sahel and in particular of the TEJ intensity. The strength of the TEJ in turn modulates upper-level divergence and the vertical zonal wind shear, and hence convection over the region (Nicholson 2009; Whittleston et al. 2017). The Niño3.4 index produces more intense rainfall modulation over Central Sahel, and therefore seems responsible for the spatial signature of monsoon rainfall change over the Sahel (Fig.S8).

Accepted for publication in *Journal of Climate*. DOI 10.1175/JCLI-D-23-0162.1.

3. How much uncertainty can they explain?

Although the two sources of uncertainty are not significantly correlated, we demonstrate that there are nevertheless plausible physical interactions between them, notably mediated by the strength of the subtropical anticyclone in the southeast Pacific. These interactions account for 12% of the uncertainty of rainfall change in the Sahel according to a bilinear regression model. However, by using attribution methods, we were able to distribute this share between the two indices and, finally, estimate their respective full contributions. Of the 62% of the inter-model spread of rainfall change in the Sahel explained by the bilinear regression: 40% are explained by the inter-hemispheric gradient and 22% by Niño3.4. The overall performance of the bilinear model is equivalent to what is obtained from the multivariate MCA optimization, and is, thus, unlikely to be further significantly improved by using only linear relationships and surface temperature indices.

Accepted for publication in *Journal of Climate*. DOI 10.1175/JCLI-D-23-0162.1.

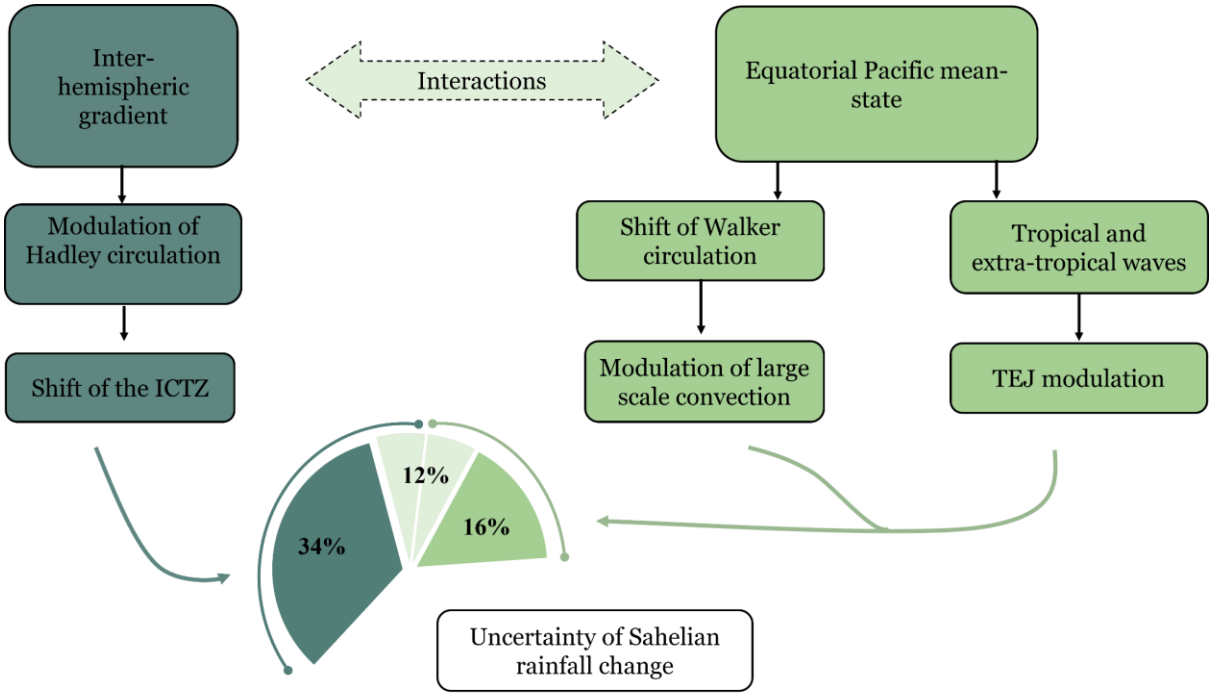

Fig. 9. Schematic diagram showing the processes by which the inter-hemispheric gradient and Niño3.4 anomalous warming patterns modulate the inter-model spread of Sahel rainfall change and their respective contributions to this inter-model spread.

The relationship between the inter-hemispheric gradient, equatorial Pacific SST and Sahel rainfall change could be further tested using SST nudging experiments. Further understanding of the mechanisms could also be obtained by using a moisture budget analysis (Chou et al. 2009; Chen et al. 2020). As our study focused on the sources of uncertainty in Sahel monsoon change under the SSP5-8.5 scenario, assessing the stationarity of relationships across the different scenarios, and between the observed and future period, would pave the way for the development of emergent constraints (Yan et al. 2019). Regarding its key role in Sahel rainfall uncertainty and its importance for global climate, further work should focus on the inter-hemispheric temperature gradient change and the radiative imbalance between the two hemispheres during boreal summer (Voigt et al. 2014). Chung and Soden (2017) and Kay et al. (2016) showed that by modulating cloud properties, anthropogenic aerosol can be critical in shaping future inter-hemispheric temperature change at least in near future. A future study should also address the sources of uncertainty in SST change in the equatorial Pacific as it plays a pivotal role in the tropical teleconnections. Such uncertainties have been linked to model

Accepted for publication in *Journal of Climate*. DOI 10.1175/JCLI-D-23-0162.1.

biases in the Pacific itself (Guilbert et al. 2023) or to biases in other basins (McGregor et al. 2018; Marathe et al. 2021; Terray et al. 2021), with equatorial undercurrent and inter-basin interactions suggested to be key to reduce these models biases (Coats and Karnauskas 2017). Furthermore, as we have so far mainly used interannual to decadal variability mechanisms to link our indices to Sahel rainfall change, improving present day performance at simulating Sahel rainfall variability could be critical to further reduce the disagreement between models projections and predictions. Finally, a storyline approach based on our results and analogous to Monerie et al. (2023) could prove highly relevant for impact studies, enabling the selection of models to sample different impact possibilities in relation to global change uncertainty.

Acknowledgments.

We thank the editor Isla Ruth Simpson as well as the two anonymous reviewers for their relevant remarks that have allowed us to improve our study. Pascal Terray and Juliette Mignot are funded by Institut de Recherche pour le Développement (IRD, France) and supported by ANR-19-JPOC-003 JPI climate/JPI ocean ROADMAP. Analysis was done with Python (https://www.python.org/) and the STATPACK and NCSTAT softwares (https://pagesperso.locean-ipsl.upmc.fr/terray/software.html). This work benefited from the ESPRI computing and data centre (https://mesocentre.ipsl.fr) which is supported by CNRS, Sorbonne University, Ecole Polytechnique and CNES and through national and international grants.

Data Availability Statement.

The study is based on the outputs of CMIP6. These are publicly available upon registration on the Data Portal of the Earth System Grid Foundation (ESGF: https://esgf-node.ipsl.upmc.fr/search/cmip6-ipsl/). ERA-Interim publicly accessible upon registration on the ECMWF Data Portal (http://apps.ecmwf.int/). The GPCP data are publicly accessible (https://psl.noaa.gov/data/gridded/data.gpcp.html).

Accepted for publication in *Journal of Climate*. DOI 10.1175/JCLI-D-23-0162.1.

REFERENCES

Adler, R. F., and Coauthors, 2003: The Version-2 Global Precipitation Climatology Project (GPCP) Monthly Precipitation Analysis (1979–Present). *J. Hydrometeorol.*, **4**, 1147–1167, https://doi.org/10.1175/1525-7541(2003)004<1147:TVGPCP>2.0.CO;2.

Akinsanola, A. A., and W. Zhou, 2019: Ensemble-based CMIP5 simulations of West African summer monsoon rainfall: current climate and future changes. *Theor. Appl. Climatol.*, **136**, 1021–1031, https://doi.org/10.1007/s00704-018-2516-3.

Almazroui, M., F. Saeed, S. Saeed, M. Nazrul Islam, M. Ismail, N. A. B. Klutse, and M. H. Siddiqui, 2020: Projected Change in Temperature and Precipitation Over Africa from CMIP6. *Earth Syst. Environ.*, **4**, 455–475, https://doi.org/10.1007/s41748-020-00161-x.

Azen, R., and D. Budescu, 2003: The Dominance Analysis Approach for Comparing Predictors in Multiple Regression. *Psychol. Methods*, **8**, 129–148, https://doi.org/10.1037/1082-989X.8.2.129.

Bellomo, K., M. Angeloni, S. Corti, and J. von Hardenberg, 2021: Future climate change shaped by inter-model differences in Atlantic meridional overturning circulation response. *Nat. Commun.*, **12**, 3659, https://doi.org/10.1038/s41467-021-24015-w.

Biasutti, M., 2013: Forced Sahel rainfall trends in the CMIP5 archive. *J. Geophys. Res. Atmospheres*, **118**, 1613–1623, https://doi.org/10.1002/jgrd.50206.

Biasutti, M., 2019: Rainfall trends in the African Sahel: Characteristics, processes, and causes. *WIREs Clim. Change*, **10**, e591, https://doi.org/10.1002/wcc.591.

Biasutti, M., I. M. Held, A. H. Sobel, and A. Giannini, 2008: SST Forcings and Sahel Rainfall Variability in Simulations of the Twentieth and Twenty-First Centuries. *J. Clim.*, **21**, 3471–3486, https://doi.org/10.1175/2007JCLI1896.1.

Biasutti, M., and Coauthors, 2018: Global energetics and local physics as drivers of past, present and future monsoons. *Nat. Geosci.*, **11**, 392–400, https://doi.org/10.1038/s41561-018-0137-1.

Bickle, M. E., J. H. Marsham, A. N. Ross, D. P. Rowell, D. J. Parker, and C. M. Taylor, 2021: Understanding mechanisms for trends in Sahelian squall lines: Roles of thermodynamics and shear. *Q. J. R. Meteorol. Soc.*, **147**, 983–1006, https://doi.org/10.1002/qj.3955.

Breiman, L., 2001: Random Forests. *Mach. Learn.*, **45**, 5–32, https://doi.org/10.1023/A:1010933404324.

Bretherton, C. S., C. Smith, and J. M. Wallace, 1992: An intercomparison of methods for

Accepted for publication in *Journal of Climate*. DOI 10.1175/JCLI-D-23-0162.1.

finding coupled patterns in climate data. *J. Clim.*, **5**, 541–560, https://doi.org/10.1175/1520-0442(1992)005<0541:AIOMFF>2.0.CO;2.

Byrne, M. P., A. G. Pendergrass, A. D. Rapp, and K. R. Wodzicki, 2018: Response of the Intertropical Convergence Zone to Climate Change: Location, Width, and Strength. *Curr. Clim. Change Rep.*, **4**, 355–370, https://doi.org/10.1007/s40641-018-0110-5.

Chang, P., L. Ji, and H. Li, 1997: A decadal climate variation in the tropical Atlantic Ocean from thermodynamic air-sea interactions. *Nature*, **385**, 516–518, https://doi.org/10.1038/385516a0.

Charney, J., P. H. Stone, and W. J. Quirk, 1975: Drought in the Sahara: A Biogeophysical Feedback Mechanism. *Science*, **187**, 434–435, https://doi.org/10.1126/science.187.4175.434.

Chen, Z., T. Zhou, L. Zhang, X. Chen, W. Zhang, and J. Jiang, 2020: Global land monsoon precipitation changes in CMIP6 projections. *Geophys. Res. Lett.*, **47**, e2019GL086902, https://doi.org/10.1029/2019GL086902.

Cherchi, A., P. Terray, S. B Ratna, S. Sankar, K. Sooraj, and S. Behera, 2021: Indian Ocean Dipole influence on Indian summer monsoon and ENSO: A review.

Cherry, S., 1997: Some comments on singular value decomposition analysis. *J. Clim.*, **10**, 1759–1761, https://doi.org/10.1175/1520-0442(1997)010<1759:SCOSVD>2.0.CO;2.

Chiang, J. C. H., and D. J. Vimont, 2004: Analogous Pacific and Atlantic Meridional Modes of Tropical Atmosphere–Ocean Variability. *J. Clim.*, **17**, 4143–4158, https://doi.org/10.1175/JCLI4953.1.

Chou, C., and J. D. Neelin, 2004: Mechanisms of Global Warming Impacts on Regional Tropical Precipitation. *J. Clim.*, **17**, 2688–2701, https://doi.org/10.1175/1520-0442(2004)017<2688:MOGWIO>2.0.CO;2.

——, J.-Y. Tu, and J.-Y. Yu, 2003: Interannual Variability of the Western North Pacific Summer Monsoon: Differences between ENSO and Non-ENSO Years. *J. Clim.*, **16**, 2275–2287, https://doi.org/10.1175/2761.1.

——, J. D. Neelin, C.-A. Chen, and J.-Y. Tu, 2009: Evaluating the “Rich-Get-Richer” Mechanism in Tropical Precipitation Change under Global Warming. *J. Clim.*, **22**, 1982–2005, https://doi.org/10.1175/2008JCLI2471.1.

Chung, E.-S., and B. Soden, 2017: Hemispheric climate shifts driven by anthropogenic aerosol–cloud interactions. *Nat. Geosci.*, **10**, https://doi.org/10.1038/ngeo2988.

Coats, S., and K. Karnauskas, 2017: Are simulated and observed 20 th century tropical Pacific sea surface temperature trends significant relative to internal variability?: Tropical Pacific SST trends in CGCMs. *Geophys. Res. Lett.*, **44**, https://doi.org/10.1002/2017GL074622.

Cook, K. H., and E. K. Vizy, 2015: Detection and Analysis of an Amplified Warming of the Sahara Desert. *J. Clim.*, **28**, 6560–6580, https://doi.org/10.1175/JCLI-D-14-00230.1.

Crétat, J., P. Terray, S. Masson, K. P. Sooraj, and M. K. Roxy, 2017: Indian Ocean and

Accepted for publication in *Journal of Climate*. DOI 10.1175/JCLI-D-23-0162.1.

Indian summer monsoon: relationships without ENSO in ocean–atmosphere coupled simulations. *Clim. Dyn.*, **49**, 1429–1448, https://doi.org/10.1007/s00382-016-3387-x.

Dee, D. P., and Coauthors, 2011: The ERA-Interim reanalysis: configuration and performance of the data assimilation system. *Q. J. R. Meteorol. Soc.*, **137**, 553–597, https://doi.org/10.1002/qj.828.

Dixon, R. D., D. J. Vimont, and A. S. Daloz, 2018: The relationship between tropical precipitation biases and the Saharan heat low bias in CMIP5 models. *Clim. Dyn.*, **50**, 3729–3744, https://doi.org/10.1007/s00382-017-3838-z.

Dong, B., and R. Sutton, 2015: Dominant role of greenhouse-gas forcing in the recovery of Sahel rainfall. *Nat. Clim. Change*, **5**, 757–760, https://doi.org/10.1038/nclimate2664.

Douville, H., D. Salas-Mélia, and S. Tyteca, 2006: On the tropical origin of uncertainties in the global land precipitation response to global warming. *Clim. Dyn.*, **26**, 367–385, https://doi.org/10.1007/s00382-005-0088-2.

Eyring, V., S. Bony, G. A. Meehl, C. A. Senior, B. Stevens, R. J. Stouffer, and K. E. Taylor, 2016: Overview of the Coupled Model Intercomparison Project Phase 6 (CMIP6) experimental design and organization. *Geosci. Model Dev.*, **9**, 1937–1958, https://doi.org/10.5194/gmd-9-1937-2016.

Fisher, A., C. Rudin, and F. Dominici, 2019: All Models are Wrong, but Many are Useful: Learning a Variable's Importance by Studying an Entire Class of Prediction Models Simultaneously. https://doi.org/10.48550/arXiv.1801.01489.

Fredriksen, H.-B., J. Berner, A. C. Subramanian, and A. Capotondi, 2020: How Does El Niño–Southern Oscillation Change Under Global Warming—A First Look at CMIP6. *Geophys. Res. Lett.*, **47**, e2020GL090640, https://doi.org/10.1029/2020GL090640.

Gaetani, M., C. Flamant, S. Bastin, S. Janicot, C. Lavaysse, F. Hourdin, P. Braconnot, and S. Bony, 2017: West African monsoon dynamics and precipitation: the competition between global SST warming and CO2 increase in CMIP5 idealized simulations. *Clim. Dyn.*, **48**, 1353–1373, https://doi.org/10.1007/s00382-016-3146-z.

García-Serrano, J., C. Cassou, H. Douville, A. Giannini, and F. J. Doblas-Reyes, 2017: Revisiting the ENSO Teleconnection to the Tropical North Atlantic. *J. Clim.*, **30**, 6945–6957, https://doi.org/10.1175/JCLI-D-16-0641.1.

Giannini, A., and A. Kaplan, 2019: The role of aerosols and greenhouse gases in Sahel drought and recovery. *Clim. Change*, **152**, 449–466, https://doi.org/10.1007/s10584-018-2341-9.

Gill, A. E., 1980: Some simple solutions for heat-induced tropical circulation. *Q. J. R. Meteorol. Soc.*, **106**, 447–462, https://doi.org/10.1002/qj.49710644905.

Grodsky, S. A., J. A. Carton, and S. Nigam, 2003: Near surface westerly wind jet in the Atlantic ITCZ. *Geophys. Res. Lett.*, **30**, https://doi.org/10.1029/2003GL017867.

Guilbert, M., P. Terray, and J. Mignot, 2023: Intermodel spread of historical Indian monsoon rainfall change in CMIP6: The role of the tropical Pacific mean-state. *J. Clim.*, **1**, 1–42, https://doi.org/10.1175/JCLI-D-22-0585.1.

Accepted for publication in *Journal of Climate*. DOI 10.1175/JCLI-D-23-0162.1.

Hawcroft, M., J. M. Haywood, M. Collins, A. Jones, A. C. Jones, and G. Stephens, 2017: Southern Ocean albedo, inter-hemispheric energy transports and the double ITCZ: global impacts of biases in a coupled model. *Clim. Dyn.*, **48**, 2279–2295, https://doi.org/10.1007/s00382-016-3205-5.

Haywood, J. M., and Coauthors, 2016: The impact of equilibrating hemispheric albedos on tropical performance in the HadGEM2-ES coupled climate model. *Geophys. Res. Lett.*, **43**, 395–403, https://doi.org/10.1002/2015GL066903.

Held, I. M., T. L. Delworth, J. Lu, K. L. Findell, and T. R. Knutson, 2005: Simulation of Sahel drought in the 20th and 21st centuries. *Proc. Natl. Acad. Sci.*, **102**, 17891–17896, https://doi.org/10.1073/pnas.0509057102.

Hill, S., 2019: Theories for Past and Future Monsoon Rainfall Changes. *Curr. Clim. Change Rep.*, **5**, 1–12, https://doi.org/10.1007/s40641-019-00137-8.

Hirasawa, H., P. Kushner, M. Sigmond, J. Fyfe, and C. Deser, 2020: Anthropogenic Aerosols Dominate Forced Multidecadal Sahel Precipitation Change through Distinct Atmospheric and Oceanic Drivers. *J. Clim.*, **33**, 1–56, https://doi.org/10.1175/JCLI-D-19-0829.1.

Hwang, Y.-T., D. M. W. Frierson, and S. M. Kang, 2013: Anthropogenic sulfate aerosol and the southward shift of tropical precipitation in the late 20th century. *Geophys. Res. Lett.*, **40**, 2845–2850, https://doi.org/10.1002/grl.50502.

Janicot, S., and Coauthors, 2011: Intraseasonal variability of the West African monsoon. *Atmospheric Sci. Lett.*, **12**, 58–66, https://doi.org/10.1002/asl.280.

Janicot, S., and Coauthors, 2015: The Recent Partial Recovery in Sahel Rainfall: A Fingerprint of Greenhouse Gases Forcing? *GEWEX News*, **27**, 11–15.

Jiang, X., T. Li, and B. Wang, 2004: Structures and Mechanisms of the Northward Propagating Boreal Summer Intraseasonal Oscillation. *J. Clim.*, **17**, 1022–1039, https://doi.org/10.1175/1520-0442(2004)017<1022:SAMOTN>2.0.CO;2.

Joly, M., and A. Voldoire, 2009: Influence of ENSO on the West African Monsoon: Temporal Aspects and Atmospheric Processes. *J. Clim.*, **22**, 3193–3210, https://doi.org/10.1175/2008JCLI2450.1.

Kay, J. E., C. Wall, V. Yettella, B. Medeiros, C. Hannay, P. Caldwell, and C. Bitz, 2016: Global Climate Impacts of Fixing the Southern Ocean Shortwave Radiation Bias in the Community Earth System Model (CESM). *J. Clim.*, **29**, 4617–4636, https://doi.org/10.1175/JCLI-D-15-0358.1.

Kent, C., R. Chadwick, and D. P. Rowell, 2015: Understanding Uncertainties in Future Projections of Seasonal Tropical Precipitation. *J. Clim.*, **28**, 4390–4413, https://doi.org/10.1175/JCLI-D-14-00613.1.

Kucharski, F., N. Zeng, and E. Kalnay, 2013: A further assessment of vegetation feedback on decadal Sahel rainfall variability. *Clim. Dyn.*, **40**, 1453–1466, https://doi.org/10.1007/s00382-012-1397-x.

Accepted for publication in *Journal of Climate*. DOI 10.1175/JCLI-D-23-0162.1.

Lebel, T., and A. Ali, 2009: Recent trends in the Central and Western Sahel rainfall regime (1990–2007). *J. Hydrol.*, **375**, 52–64, https://doi.org/10.1016/j.jhydrol.2008.11.030.

Li, G., S.-P. Xie, C. He, and Z. Chen, 2017: Western Pacific emergent constraint lowers projected increase in Indian summer monsoon rainfall. *Nat. Clim. Change*, **7**, 708–712, https://doi.org/10.1038/nclimate3387.

Lian, T., D. Chen, J. Ying, P. Huang, and Y. Tang, 2019: Tropical Pacific trends under global warming: El Niño-like or La Niña-like? *Natl. Sci. Rev.*, **5**, https://doi.org/10.1093/nsr/nwy134.

Madhavan, M., L. Ravisankar, K. Thirumalai, and R. Ramesh, 2022: Coherent Indian Summer Monsoon and Sahel Rainfall Variability Revealed by Ethiopian Rainfall δ 18 O. *J. Geophys. Res. Atmospheres*, **127**, https://doi.org/10.1029/2022JD037160.

Marathe, S., P. Terray, and A. Karumuri, 2021: Tropical Indian Ocean and ENSO relationships in a changed climate. *Clim. Dyn.*, **56**, 3255–3276, https://doi.org/10.1007/s00382-021-05641-y.

Martin, E. R., and C. D. Thorncroft, 2014: The impact of the AMO on the West African monsoon annual cycle. *Q. J. R. Meteorol. Soc.*, **140**, 31–46, https://doi.org/10.1002/qj.2107.

——, C. Thorncroft, and B. B. B. Booth, 2014: The Multidecadal Atlantic SST—Sahel Rainfall Teleconnection in CMIP5 Simulations. *J. Clim.*, **27**, 784–806, https://doi.org/10.1175/JCLI-D-13-00242.1.

Marvel, K., M. Biasutti, and C. Bonfils, 2020: Fingerprints of external forcings on Sahel rainfall: aerosols, greenhouse gases, and model-observation discrepancies. *Environ. Res. Lett.*, **15**, 084023, https://doi.org/10.1088/1748-9326/ab858e.

McGregor, S., M. F. Stuecker, J. B. Kajtar, M. H. England, and M. Collins, 2018: Model tropical Atlantic biases underpin diminished Pacific decadal variability. *Nat. Clim. Change*, **8**, 493–498, https://doi.org/10.1038/s41558-018-0163-4.

Meehl, G. A., C. A. Senior, V. Eyring, G. Flato, J.-F. Lamarque, R. J. Stouffer, K. E. Taylor, and M. Schlund, 2020: Context for interpreting equilibrium climate sensitivity and transient climate response from the CMIP6 Earth system models. *Sci. Adv.*, **6**, eaba1981, https://doi.org/10.1126/sciadv.aba1981.

Monerie, P.-A., B. Fontaine, and P. Roucou, 2013: Mid-century effects of Climate Change on African monsoon dynamics using the A1B emission scenario. *Int. J. Climatol.*, **33**, 881–896, https://doi.org/10.1002/joc.3476.

——, E. Sanchez-Gomez, and J. Boé, 2017a: On the range of future Sahel precipitation projections and the selection of a sub-sample of CMIP5 models for impact studies. *Clim. Dyn.*, **48**, 2751–2770, https://doi.org/10.1007/s00382-016-3236-y.

——, ——, B. Pohl, J. Robson, and B. Dong, 2017b: Impact of internal variability on projections of Sahel precipitation change. *Environ. Res. Lett.*, **12**, 114003, https://doi.org/10.1088/1748-9326/aa8cda.

——, ——, M. Gaetani, E. Mohino, and B. Dong, 2020a: Future evolution of the Sahel

Accepted for publication in *Journal of Climate*. DOI 10.1175/JCLI-D-23-0162.1.

precipitation zonal contrast in CESM1. *Clim. Dyn.*, **55**, 2801–2821, https://doi.org/10.1007/s00382-020-05417-w.

——, C. M. Wainwright, M. Sidibe, and A. A. Akinsanola, 2020b: Model uncertainties in climate change impacts on Sahel precipitation in ensembles of CMIP5 and CMIP6 simulations. *Clim. Dyn.*, **55**, 1385–1401, https://doi.org/10.1007/s00382-020-05332-0.

——, B. Pohl, and M. Gaetani, 2021: The fast response of Sahel precipitation to climate change allows effective mitigation action. *Npj Clim. Atmospheric Sci.*, **4**, 1–8, https://doi.org/10.1038/s41612-021-00179-6.

——, L. J. Wilcox, and A. G. Turner, 2022: Effects of Anthropogenic Aerosol and Greenhouse Gas Emissions on Northern Hemisphere Monsoon Precipitation: Mechanisms and Uncertainty. *J. Clim.*, **35**, 2305–2326, https://doi.org/10.1175/JCLI-D-21-0412.1.

——, M. Biasutti, J. Mignot, E. Mohino, B. Pohl, and G. Zappa, 2023: Storylines of Sahel Precipitation Change: Roles of the North Atlantic and Euro-Mediterranean Temperature. *J. Geophys. Res. Atmospheres*, **128**, e2023JD038712, https://doi.org/10.1029/2023JD038712.

Nakanishi, T., Y. Tachibana, and Y. Ando, 2021: Possible semi-circumglobal teleconnection across Eurasia driven by deep convection over the Sahel. *Clim. Dyn.*, **57**, 2287–2299, https://doi.org/10.1007/s00382-021-05804-x.

Ndiaye, C. D., E. Mohino, J. Mignot, and S. M. Sall, 2022: On the Detection of Externally Forced Decadal Modulations of the Sahel Rainfall over the Whole Twentieth Century in the CMIP6 Ensemble. *J. Clim.*, **35**, 3339–3354, https://doi.org/10.1175/JCLI-D-21-0585.1.

Nicholson, S., 2013a: The West African Sahel: A Review of Recent Studies on the Rainfall Regime and Its Interannual Variability. *ISRN Meteorol.*, **2013**, https://doi.org/10.1155/2013/453521.

Nicholson, S. E., 2009: A revised picture of the structure of the “monsoon” and land ITCZ over West Africa. *Clim. Dyn.*, **32**, 1155–1171, https://doi.org/10.1007/s00382-008-0514-3.

——, 2013b: The West African Sahel: A Review of Recent Studies on the Rainfall Regime and Its Interannual Variability. *Int. Sch. Res. Not.*, **2013**, e453521, https://doi.org/10.1155/2013/453521.

Park, J., J. Bader, and D. Matei, 2016: Anthropogenic Mediterranean warming essential driver for present and future Sahel rainfall. *Nat. Clim. Change*, **6**, 941–945, https://doi.org/10.1038/nclimate3065.

Park, J.-Y., J. Bader, and D. Matei, 2015: Northern-hemispheric differential warming is the key to understanding the discrepancies in the projected Sahel rainfall. *Nat. Commun.*, **6**, 5985, https://doi.org/10.1038/ncomms6985.

Pascale, S., W. R. Boos, S. Bordoni, T. L. Delworth, S. B. Kapnick, H. Murakami, G. A. Vecchi, and W. Zhang, 2017: Weakening of the North American monsoon with global warming. *Nat. Clim. Change*, **7**, 806–812, https://doi.org/10.1038/nclimate3412.

Accepted for publication in *Journal of Climate*. DOI 10.1175/JCLI-D-23-0162.1.

Pu, B., and K. H. Cook, 2010: Dynamics of the West African Westerly Jet. *J. Clim.*, **23**, 6263–6276, https://doi.org/10.1175/2010JCLI3648.1.

——, and ——, 2012: Role of the West African Westerly Jet in Sahel Rainfall Variations. *J. Clim.*, **25**, 2880–2896, https://doi.org/10.1175/JCLI-D-11-00394.1.

Roehrig, R., D. Bouniol, F. Guichard, F. Hourdin, and J.-L. Redelsperger, 2013: The Present and Future of the West African Monsoon: A Process-Oriented Assessment of CMIP5 Simulations along the AMMA Transect. *J. Clim.*, **26**, 6471–6505, https://doi.org/10.1175/JCLI-D-12-00505.1.

Roy, I., R. G. Tedeschi, and M. Collins, 2019: ENSO teleconnections to the Indian summer monsoon under changing climate. *Int. J. Climatol.*, **39**, 3031–3042, https://doi.org/10.1002/joc.5999.

Sathiyamoorthy, V., 2005: Large scale reduction in the size of the Tropical Easterly Jet. *Geophys. Res. Lett.*, **32**, https://doi.org/10.1029/2005GL022956.

Schneider, T., T. Bischoff, and G. H. Haug, 2014: Migrations and dynamics of the intertropical convergence zone. *Nature*, **513**, 45–53, https://doi.org/10.1038/nature13636.

Seth, A., A. Giannini, M. Rojas, S. A. Rauscher, S. Bordoni, D. Singh, and S. J. Camargo, 2019: Monsoon responses to climate changes—connecting past, present and future. *Curr. Clim. Change Rep.*, **5**, 63–79, https://doi.org/10.1007/s40641-019-00125-y.

Shaman, J., and E. Tziperman, 2007: Summertime ENSO–North African–Asian Jet teleconnection and implications for the Indian monsoons. *Geophys. Res. Lett.*, **34**, https://doi.org/10.1029/2006GL029143.

Shekhar, R., and W. R. Boos, 2017: Weakening and Shifting of the Saharan Shallow Meridional Circulation during Wet Years of the West African Monsoon. *J. Clim.*, **30**, 7399–7422, https://doi.org/10.1175/JCLI-D-16-0696.1.

Sooraj, K. P., P. Terray, S. Masson, and J. Crétat, 2019: Modulations of the Indian summer monsoon by the hot subtropical deserts: insights from coupled sensitivity experiments. *Clim. Dyn.*, **52**, 4527–4555, https://doi.org/10.1007/s00382-018-4396-8.

Su, J., R. Zhang, T. Li, X. Rong, J.-S. Kug, and C.-C. Hong, 2010: Causes of the El Niño and La Niña Amplitude Asymmetry in the Equatorial Eastern Pacific. *J. Clim.*, **23**, 605–617, https://doi.org/10.1175/2009JCLI2894.1.

Sultan, B., and S. Janicot, 2003: The West African Monsoon Dynamics. Part II: The “Preonset” and “Onset” of the Summer Monsoon. *J. Clim.*, **16**, 3407–3427, https://doi.org/10.1175/1520-0442(2003)016<3407:TWAMDP>2.0.CO;2.

——, and M. Gaetani, 2016: Agriculture in West Africa in the Twenty-First Century: Climate Change and Impacts Scenarios, and Potential for Adaptation. *Front. Plant Sci.*, **7**.

Sylla, M. B., P. M. Nikiema, P. Gibba, I. Kebe, and N. A. B. Klutse, 2016: Climate Change over West Africa: Recent Trends and Future Projections. *Adaptation to Climate Change and Variability in Rural West Africa*, J.A. Yaro and J. Hesselberg, Eds.,

Accepted for publication in *Journal of Climate*. DOI 10.1175/JCLI-D-23-0162.1.

Springer International Publishing, 25–40.

Tanaka, H. L., N. Ishizaki, and A. Kitoh, 2004: Trend and interannual variability of Walker, monsoon and Hadley circulations defined by velocity potential in the upper troposphere. *Tellus A*, **56**, 250–269, https://doi.org/10.1111/j.1600-0870.2004.00049.x.

Tao, W., X. Kong, L. Yong, Y. Wang, and D. Danhong, 2022: Diversity of Northwest Pacific atmospheric circulation anomalies during post-ENSO summer. *Front. Environ. Sci.*, **10**, 1068155, https://doi.org/10.3389/fenvs.2022.1068155.

Terray, P., K. P. Sooraj, S. Masson, R. P. M. Krishna, G. Samson, and A. G. Prajeesh, 2018: Towards a realistic simulation of boreal summer tropical rainfall climatology in state-of-the-art coupled models: role of the background snow-free land albedo. *Clim. Dyn.*, **50**, 3413–3439, https://doi.org/10.1007/s00382-017-3812-9.

Terray, P., K. P. Sooraj, S. Masson, and C. Prodhomme, 2021: Anatomy of the Indian Summer Monsoon and ENSO relationships in state-of-the-art CGCMs: role of the tropical Indian Ocean. *Clim. Dyn.*, **56**, 329–356, https://doi.org/10.1007/s00382-020-05484-z.

Timmermann, A., and Coauthors, 2018: El Niño–Southern Oscillation complexity. *Nature*, **559**, 535–545, https://doi.org/10.1038/s41586-018-0252-6.

Trenberth, K. E., G. W. Branstator, D. Karoly, A. Kumar, N.-C. Lau, and C. Ropelewski, 1998: Progress during TOGA in understanding and modeling global teleconnections associated with tropical sea surface temperatures. *J. Geophys. Res. Oceans*, **103**, 14291–14324, https://doi.org/10.1029/97JC01444.

Voigt, A., B. Stevens, J. Bader, and T. Mauritsen, 2014: Compensation of Hemispheric Albedo Asymmetries by Shifts of the ITCZ and Tropical Clouds. *J. Clim.*, **27**, 1029–1045, https://doi.org/10.1175/JCLI-D-13-00205.1.

Wang, B., R. Wu, and K.-M. Lau, 2001: Interannual Variability of the Asian Summer Monsoon: Contrasts between the Indian and the Western North Pacific–East Asian Monsoons. *J. Clim.*, **14**, 4073–4090, https://doi.org/10.1175/1520-0442(2001)014<4073:IVOTAS>2.0.CO;2.

Wei, N., L. Zhou, Y. Dai, G. Xia, and W. Hua, 2017: Observational evidence for desert amplification using multiple satellite datasets. *Sci. Rep.*, **7**, 2043, https://doi.org/10.1038/s41598-017-02064-w.

Whittleston, D., S. E. Nicholson, A. Schlosser, and D. Entekhabi, 2017: Climate Models Lack Jet–Rainfall Coupling over West Africa. *J. Clim.*, **30**, 4625–4632, https://doi.org/10.1175/JCLI-D-16-0579.1.

Yan, Y., R. Lu, and C. Li, 2019: Relationship between the Future Projections of Sahel Rainfall and the Simulation Biases of Present South Asian and Western North Pacific Rainfall in Summer. *J. Clim.*, **32**, 1327–1343, https://doi.org/10.1175/JCLI-D-17-0846.1.

Zelinka, M. D., T. A. Myers, D. T. McCoy, S. Po-Chedley, P. M. Caldwell, P. Ceppi, S. A. Klein, and K. E. Taylor, 2020: Causes of Higher Climate Sensitivity in CMIP6 Models. *Geophys. Res. Lett.*, **47**, e2019GL085782, https://doi.org/10.1029/2019GL085782.

Accepted for publication in *Journal of Climate*. DOI 10.1175/JCLI-D-23-0162.1.

Zhang, Z., and G. Li, 2022: Uncertainty in the projected changes of Sahel summer rainfall under global warming in CMIP5 and CMIP6 multi-model ensembles. *Clim. Dyn.*, **59**, 1–19, https://doi.org/10.1007/s00382-022-06284-3.

Accepted for publication in *Journal of Climate.* DOI 10.1175/JCLI-D-23-0162.1.